AD-A087 515 PAYNE INC ANNAPOLIS MD F/G 20/4
AFTERBODY DRAG, VOLUME 2. JET INTERFERENCE EFFECTS ON SUBSONIC --ETC(U)
JUN 80 P R PAYNE N00014-77-C-0039
UNCLASSIFIED A125-1-VOL-2 DTNSRDC/ASED-80/12-VOL-2 NL

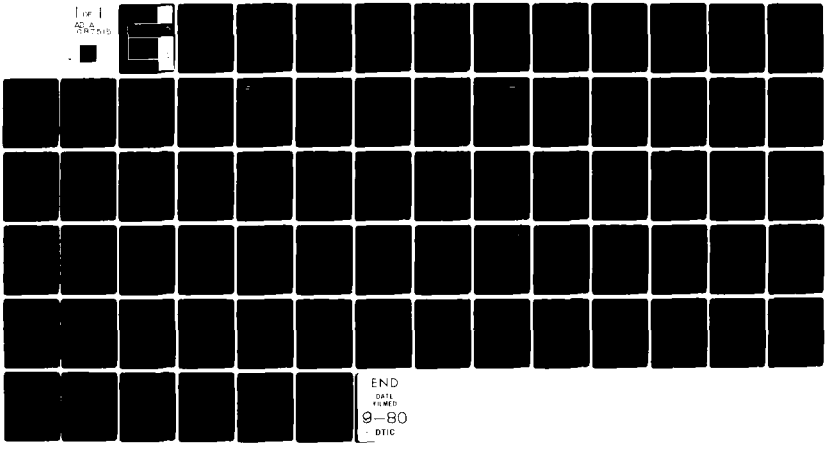

LEVEL III

AFTERBODY DRAG

VOLUME 2 – JET INTERFERENCE EFFECTS ON SUBSONIC BOATTAIL DRAG

by

Peter R. Payne
Payne, Incorporated

APPROVED FOR PUBLIC RELEASE: DISTRIBUTION UNLIMITED

AVIATION AND SURFACE EFFECTS DEPARTMENT

DTNSRDC/ASED-80/12

June 1980

DAVID W. TAYLOR NAVAL SHIP RESEARCH AND DEVELOPMENT CENTER

BETHESDA MARYLAND 20084

UNCLASSIFIED

SECURITY CLASSIFICATION OF THIS PAGE (When Data Entered)

REPORT DOCUMENTATION PAGE

READ INSTRUCTIONS BEFORE COMPLETING FORM

1. REPORT NUMBER: DTNSRDC/ASED-80/12	2. GOVT ACCESSION NO.: AD-A087 515
3. RECIPIENT'S CATALOG NUMBER:	
4. TITLE (and Subtitle): AFTERBODY DRAG, VOLUME 2, JET INTERFERENCE EFFECTS ON SUBSONIC BOTTAIL DRAG,	5. TYPE OF REPORT & PERIOD COVERED: Final Report
	6. PERFORMING ORG. REPORT NUMBER: A125-1-Vol-2
7. AUTHOR(s): Peter R. Payne	8. CONTRACT OR GRANT NUMBER(s): N00014-77-0039
9. PERFORMING ORGANIZATION NAME AND ADDRESS: Payne Incorporated, Annapolis, Maryland 21401	10. PROGRAM ELEMENT, PROJECT, TASK AREA & WORK UNIT NUMBERS: (See reverse side)
11. CONTROLLING OFFICE NAME AND ADDRESS: David W. Taylor Naval Ship R&D Center, Aviation and Surface Effects Department, Bethesda, Maryland 20084	12. REPORT DATE: June 1980
	13. NUMBER OF PAGES: 75
14. MONITORING AGENCY NAME & ADDRESS (if different from Controlling Office): Naval Air Systems Command, Washington D.C. 20361; Naval Weapons Center, China Lake, California 93555	15. SECURITY CLASS. (of this report): UNCLASSIFIED
	15a. DECLASSIFICATION/DOWNGRADING SCHEDULE

16. DISTRIBUTION STATEMENT (of this Report)

APPROVED FOR PUBLIC RELEASE: DISTRIBUTION UNLIMITED

17. DISTRIBUTION STATEMENT (of the abstract entered in Block 20, if different from Report)

18. SUPPLEMENTARY NOTES

19. KEY WORDS (Continue on reverse side if necessary and identify by block number)

Base Pressure
Boattail Drag
Jet Interference
Subsonic Flow
Transonic Flow

20. ABSTRACT (Continue on reverse side if necessary and identify by block number)

The results of the afterbody drag study are presented in four volumes, -- Volume 1: Drag of Conical and Circular Arc Afterbodies; Volume 2: Jet Interference Effects on Subsonic Boattail Drag; Volume 3: Literature Survey; and Volume 4: Data and Analysis

Volume 2 includes a method of analysis as a base from which a more detailed analysis of afterbody drag can be developed.

DD FORM 1 JAN 73 1473 EDITION OF 1 NOV 65 IS OBSOLETE
S/N 0102-LF-014-6601

UNCLASSIFIED

SECURITY CLASSIFICATION OF THIS PAGE (When Data Entered)

(Block 10)

Program Elements:
63361N
62332N
62241N

Task Area Numbers:
W15X20000
F32.322.203
WF41.421.201

Work Unit Numbers:
1660-234
1660-235

TABLE OF CONTENTS

LIST OF SYMBOLS

A	$\tan \theta$
A^*	Sonic throat area
C_p	Static pressure coefficient = $\Delta p / \frac{1}{2} \rho u_o^2$
K_v	Velocity mixing coefficient defined in equation (4)
k	Entrainment coefficient defined in equation (5)
M	Free stream Mach number u_o/a_o
M_B	Mach number of the plume boundary, equation (24)
n	Entrainment ratio defined in equation (5)
p	Local static pressure
p_E	Static pressure at the jet exit, equations (26) and (27)
p_{jt}	Total pressure in the jet
p_∞	Free-stream static pressure
Δp	$p - p_\infty$
q	Strength of an axial source or sink line per unit length
R_j	A jet plume curvature parameter, defined in Figure 19
r	Radial distance in cylindrical coordinates
r_i	Potential "core" radius, defined after equation (4)
r_j	Jet radius (see Figure 3)
r_m	Maximum body radius (see Figure 3)
u_j	Jet velocity. Generally, $u_j = u_{jo}$
u_{jo}	Jet "core" velocity, assumed uniform
u_o	Free-stream velocity
Δu	Change in fluid velocity parallel to the flow axis
v	Radial velocity in cylindrical coordinates
Δv	Change in radial fluid velocity
x	Distance along the axis of symmetry
x_j	Downstream distance from the jet exit (see Figure 3)
x_{jm}	Location of maximum plume diameter
x_1	A dummy variable
z	A transformation variable with various meanings which are defined where it is employed
α_N	Nozzle angle, defined in Figure 19
β	$\sqrt{1 - M^2}$

LIST OF SYMBOLS (continued)

γ	Ratio of specific heats
δ_j	Initial turning angle of jet, defined in Figure 19
ε	Virtual kinematic viscosity
θ	Surface angle at the jet end of the boattail (see Figure 3)
λ	$(u_j/u_o) - 1$
μ	$(k/2)\lambda$
ν	Prandtl-Meyer expansion angle defined in equations (22) and (23)
ρ	Fluid mass density
Φ	The "shape factor" defined in equations (17) and (18)
ψ	$\beta A = \beta \tan \theta$

Suffixes

βE	On the boattail, due to entrainment
βP	On the boattail, due to jet pluming
o	Free stream
j	Jet
t	Total

ABSTRACT

The results of the afterbody drag study are presented in four volumes -- Volume 1: Drag of Conical and Circular Arc Afterbodies; Volume 2: Jet Interference Effects on Subsonic Boattail Drag; Volume 3: Literature Survey; and Volume 4: Data and Analysis

Volume 2 includes a method of analysis as a base from which a more detailed analysis of afterbody drag can be developed.

ADMINISTRATIVE INFORMATION

The work reported was performed for the David W. Taylor Naval Ship Research and Development Center by Payne, Incorporated under ONR Contract N0014-77-C-0039 as part of an evaluation of afterbody drag. The afterbody drag project was supported by the Naval Air Systems Command and the Naval Weapons Center under Program Elements 63361N, 62332N, and 62241N; Task Areas W15X20000, F32.322.203, and WF41.421.201; and Work Units 1660-234 and 1660-235.

The views and conclusions contained in this document are not necessarily the official policies either expressed or implied, of the David W. Taylor Naval Ship Research and Development Center or the U.S. Government. The format of this report is that of Payne, Incorporated.

INTRODUCTION

This report is concerned with the effect of a propulsive jet upon the static pressure distribution over the boattail from which it issues, and hence its effect on the boattail drag. (We do not consider "base drag" and formally exclude it by assuming zero base area.) It is a fundamental analysis in the sense that there are no "factors determined from experiment" in the usual sense, but on the other hand, no claims to comprehensiveness are made. The work presented is offered as a basis from which a more comprehensive analysis can be developed, in that it does quantify a reasonably meaningful physical picture. The theory does not apply if the flow is separated.

Figure 1 depicts a typical variation of C_{D_β} with the jet to free stream velocity ratio, which is a function of

Nozzle pressure ratio (NPR)

Jet temperature

Ratio of specific heats in the jet (γ).

Figure 2 gives the relationship between jet Mach number M_j and NPR.

Referring to Figure 1, we see that the jet-off drag is typically high and falls rapidly when quite small quantities of fluid are allowed to flow from the nozzle. This region has been explored quite extensively, from an experimental point of view, although little theoretical analysis has been undertaken. In this region, the flow field is so different from that pertaining when the propulsive jet is present that there seems little hope of correlating the two regimes, as some writers have attempted.

The region between "base bleed" and $u_j = u_o$ has been little explored, either theoretically or experimentally, probably because it is of little practical importance. When the jet velocity equals the free stream velocity, we have the "true" boattail drag without interference. (This is an approximation because the static pressure behind the nozzle is locally a little above ambient, so the velocity is therefore a little below free stream.) Again, there is very little experimental data available for this region; perhaps because the experimentalists haven't fully appreciated its significance as a "benchmark" data point.

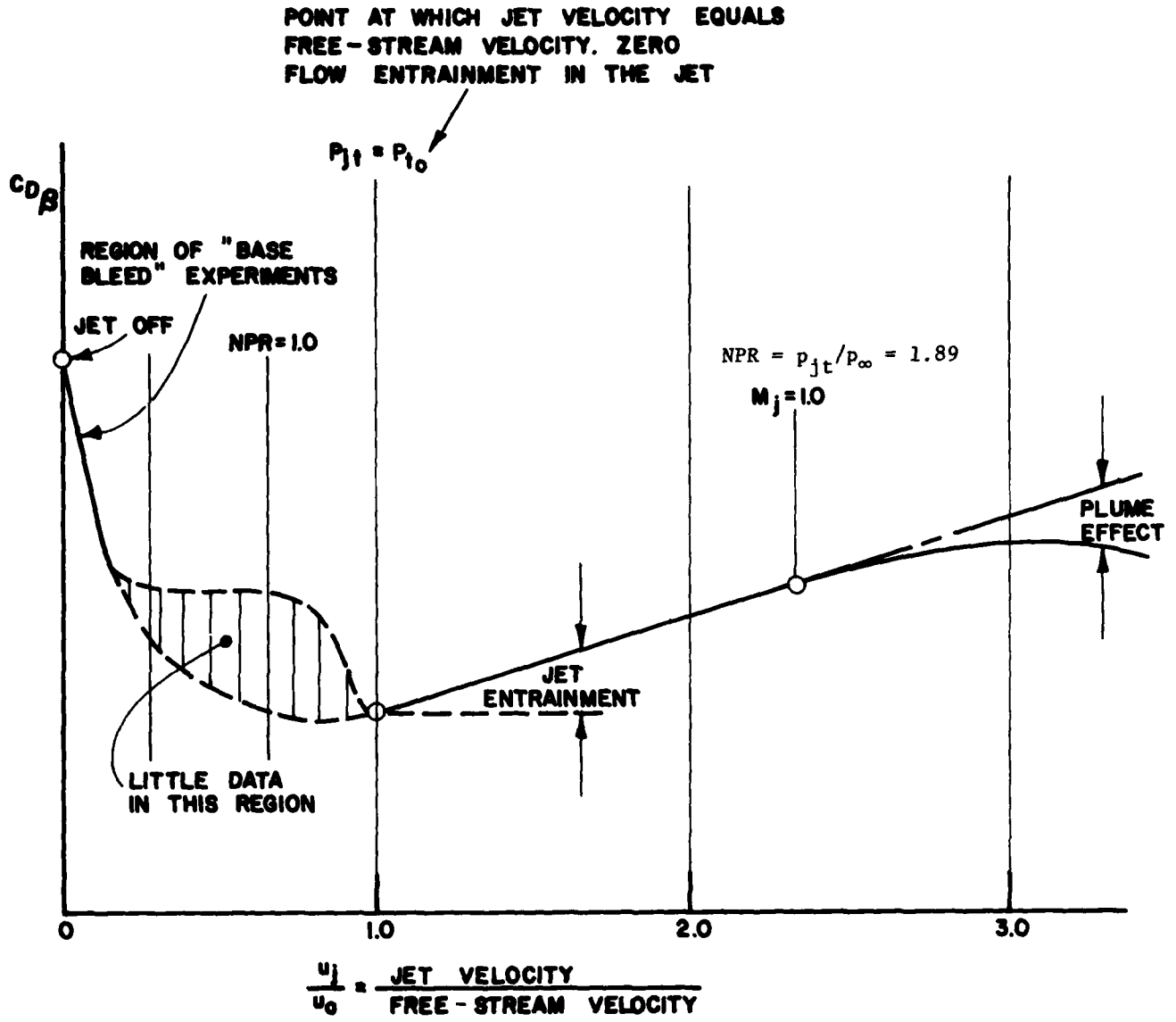

Figure 1. A Typical Variation of Boattail Drag Coefficient ($C_{D\beta}$) with Nozzle Pressure Ratio (NPR).

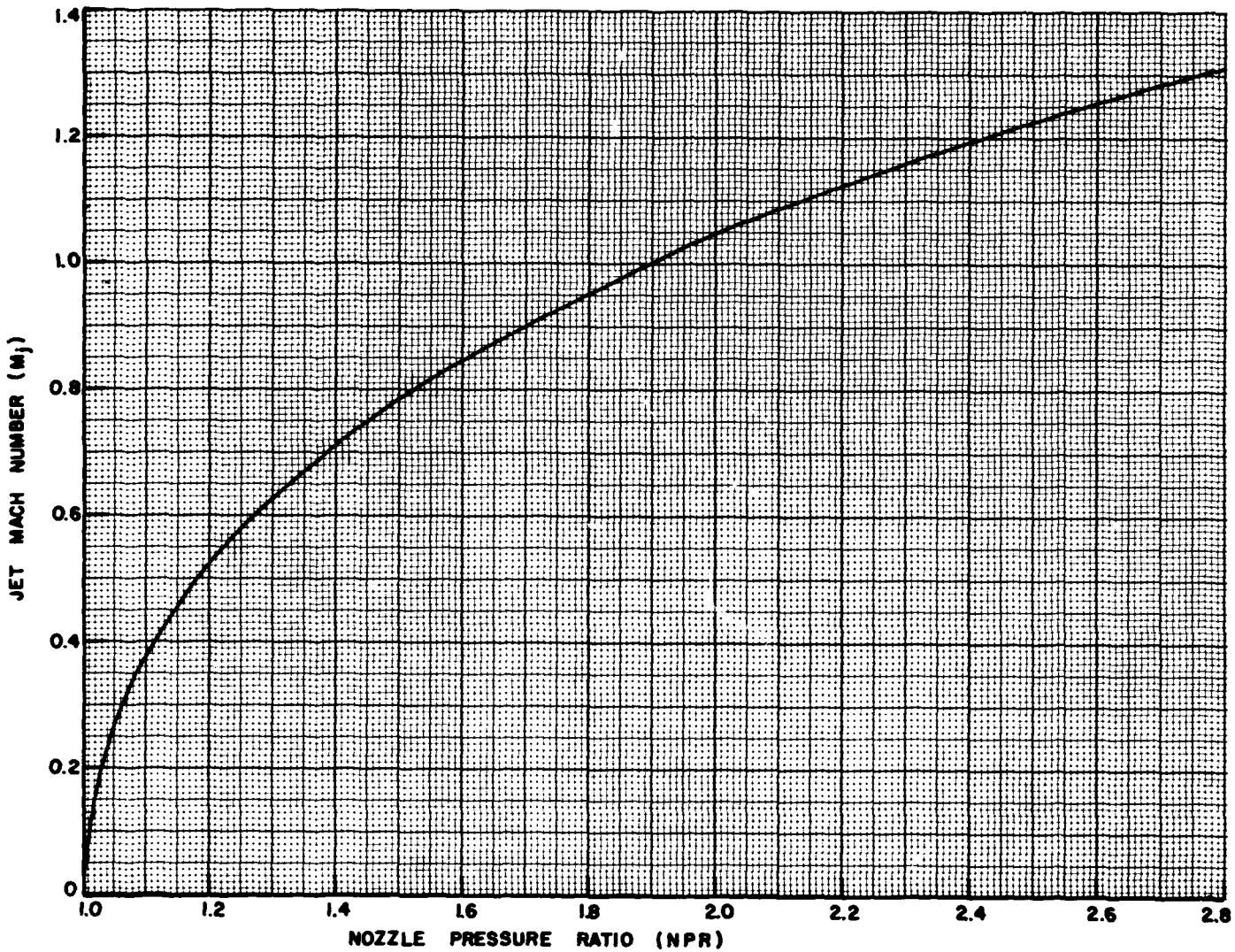

Figure 2. The Variation Between Jet Mach Number (M_j) and Nozzle Pressure Ratio (NPR) When $\gamma = 1.4$.

At higher jet velocities, free air is entrained into the jet, which therefore acts as a "sink," and increases the velocity over the boattail, and therefore its drag. The theory of this report suggests that this is a linear effect and that the boattail drag will increase linearly with jet velocity until it reaches sonic velocity. This does seem to be borne out by experiment; but in most published studies, it's rare to find even three experimental points in this region for a given configuration.

As the jet passes through sonic speed, a number of second order phenomena can cause discrepancies between one test configuration and another. The next major trend, however, is caused by the exhaust pluming, as its speed is further increased. This has the same effect as a distributed source in the wake, and reduces the flow velocity over the boattail, leading to an increase in pressure and a reduction in drag. So the plume effect starts to cancel out the drag increment due to entrainment. Eventually, the plume is large enough for the boattail drag to become negative.

The effects are most marked when there is no base area, and this is the case we have considered. A base tends to insulate the boattail from these effects, and they diminish with increasing base area. Further study is needed for the more complex case of a finite base with a jet issuing from its center.

ENTRAINMENT DRAG ON THE BOATTAIL

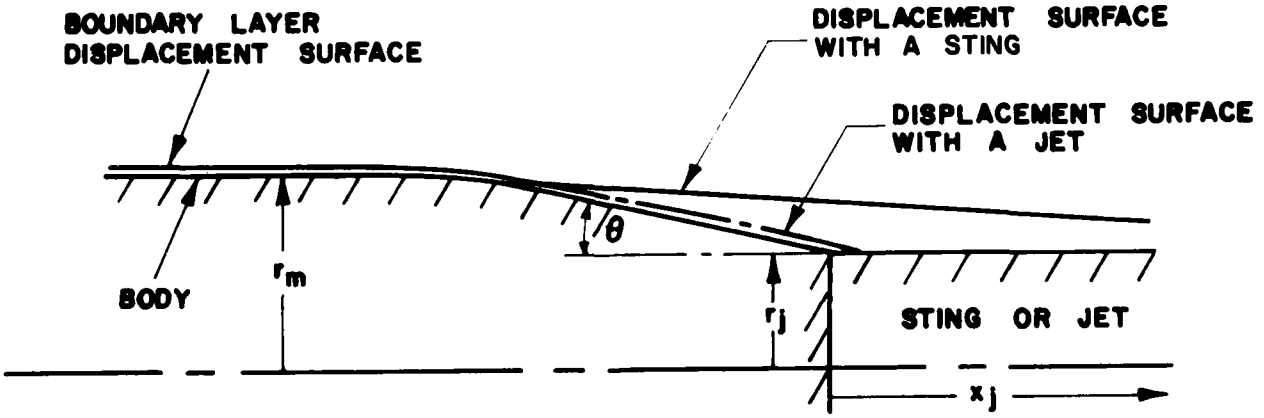

Figure 3. The Effect of Propulsive Jet Entrainment on the Boundary Layer Displacement Surface ($M_\infty \simeq 0.9$).

Figure 3 (after Grossman & Melnik[1]) shows the change in the boundary layer displacement surface when a propulsive jet replaces a sting. Figure 4 below depicts the displacement surface location for two different jet velocities; the higher the jet velocity ratio u_j/u_o, the more rapidly the boundary layer is entrained in the jet, and so the greater the suction on the afterbody. Free air entrainment by the jet also changes the static pressure distribution over the afterbody, and hence the forces acting upon it.

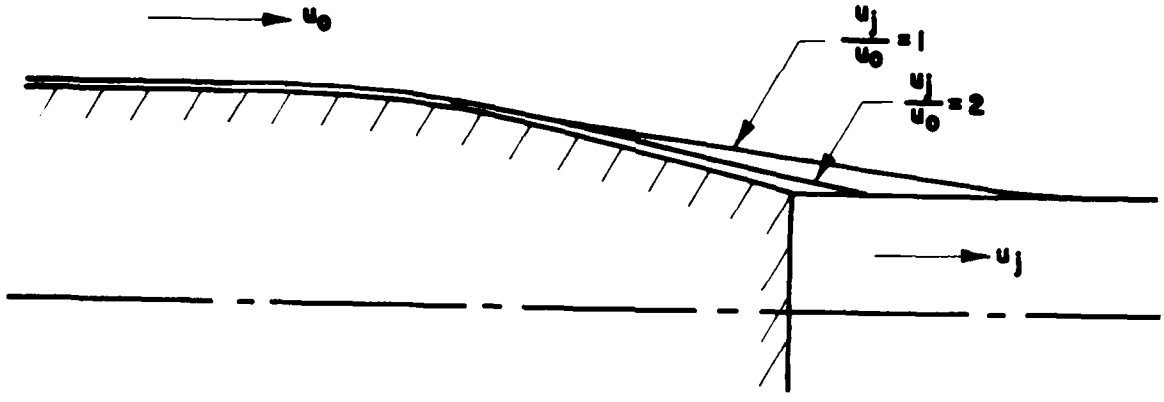

Figure 4. The Boundary Layer Displacement Surface for Two Different Jet Velocity Ratios.

This jet-induced drag effect was noted almost as soon as jet engines were applied to aircraft propulsion. Figure 5 shows some typical data obtained by Riegels and Eggert[2] in 1944.

Kuchemann and Weber[3] observed that $\Delta C_{P_{\beta E}}$ the change in the pressure coefficient C_p varied as $(u_j/u_o - 1)$ and was practically constant over the boattail, so that the pressure and drag increments due to entrainment could be written as

$$\Delta C_{P_{\beta E}} = 0.01\ (u_j/u_o - 1) \tag{1}$$

$$\left.\begin{aligned} \therefore\ C_{D_{\beta E}} &= 0.01[u_j/u_o - 1][1 - (r_j/r_m)^2] \\ \text{and} \\ \frac{\text{Drag Increase}}{\text{Jet Thrust}} &= 0.005[\rho_o/\rho_j][u_o/u_j][(r_m/r_j)^2 - 1] \end{aligned}\right\} \tag{2}$$

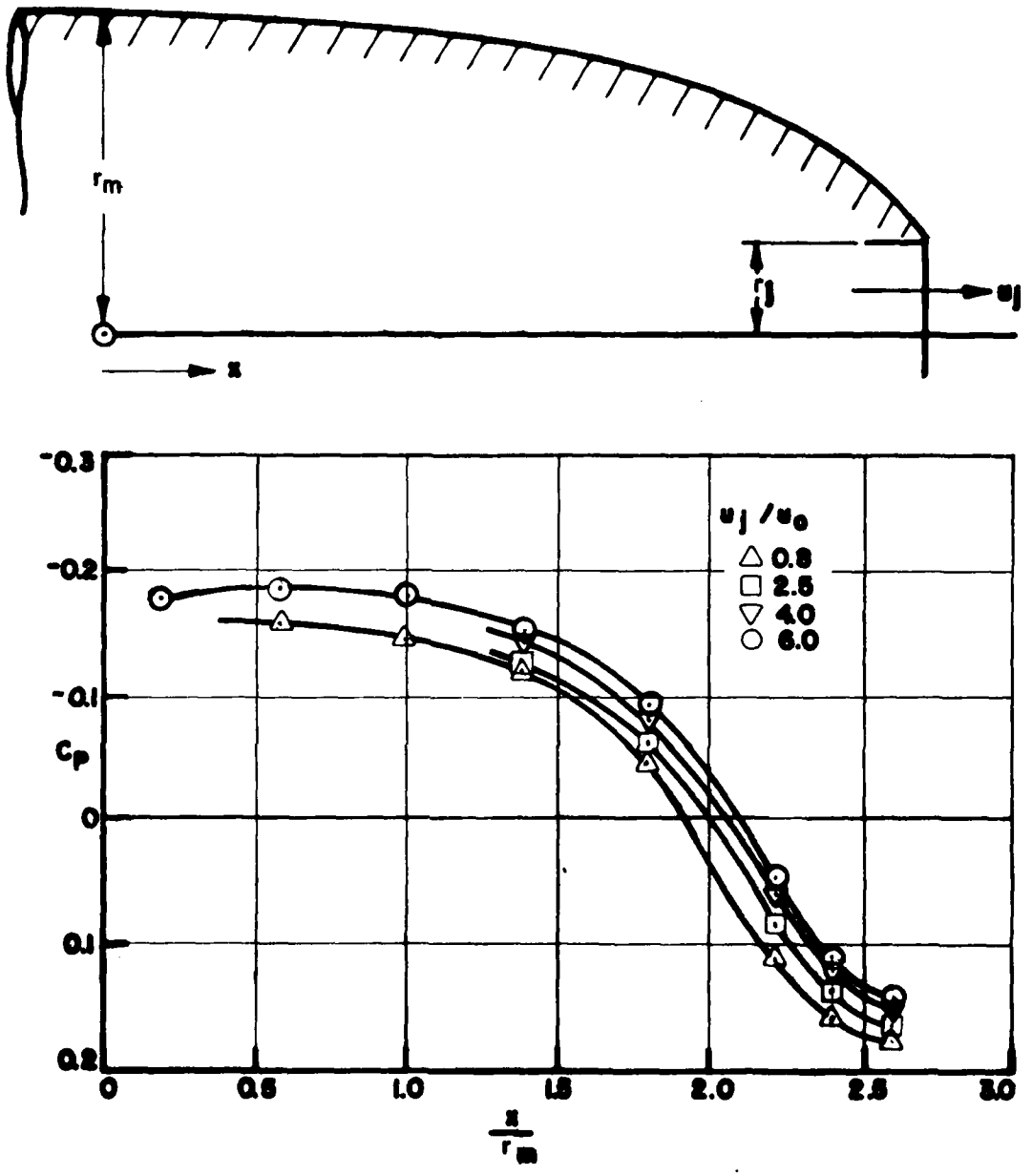

Figure 5. An Early Measurement of the Change in Boattail Static Pressure Distribution with Jet Velocity Ratio. (Ref. 2)

Kuchemann and Weber[3] suggested that the drag increase would be typically less than 1% of the thrust, so that the entrainment effect would be unimportant. This is no longer true with many modern aircraft and missile configurations, of course.

There are two alternative methods of computing the change in boattail drag due to entrainment ($C_{D_{\beta E}}$). The most time consuming is to compute, iteratively, the pressure distribution over the boattail, including the entrainment effect of the boundary layer. Without entrainment, such calculations have been carried out by many investigators. Recent examples are the papers of Grossman and Melnik[1], Moulden, Wu and Spring[4], and Chow, Bober and Anderson[5]. But such studies, while they are important to gaining a better understanding of the underlying physical processes, are not at all suitable for correlating experimental data. And, of course, additional work is needed to introduce a satisfactory model of jet entrainment.

The other approach is to employ the principle of linear superpositioning. If it is possible to describe the flow over the boattail by a suitable distribution of singularities, then the change in this flow due to other singularities can be calculated without knowing the details of the original ones, or the details of the corresponding flow field. The limitations of this approach are obvious. The displacement surface of the boundary layer can change in a nonlinear way when the external flow field is changed, and not all axisymmetric bodies can be described by singularities on their axis. So we must hope that the errors so introduced are not too large or that they are systematic and identifiable.

It seems reasonable to suppose that jet entrainment can be represented by a sink distribution in the jet, ideally a cylindrical sink surface located at the jet boundary. But since we do not know the entrainment details very accurately, a line sink distribution on the centerline axis is probably a reasonable approximation. But before attempting to define values for such a distribution, we need to describe a jet in a little more detail.

If u_o and u_{jo} are the free-stream and jet ("potential core") velocities, v the jet radial velocity, and x_j and r are cylindrical coordinates in the jet, then the equations of motion for the jet are:

$$\left.\begin{aligned} u_j \frac{\partial u_j}{\partial x_j} + v \frac{\partial u_j}{\partial r} &= \frac{\varepsilon}{r} \frac{\partial}{\partial r}\left(r \frac{\partial u_j}{\partial r}\right) \\ \frac{\partial u_j}{\partial x_j} + \frac{\partial v}{\partial r} + \frac{v}{r} &= 0 \end{aligned}\right\} \qquad (3)$$

It is usual to express the virtual kinematic viscosity ε in the form given by Prandtl's mixing length theory*

$$\varepsilon = r_j u_{jo} \frac{K_v}{2} (r_{0.5} - r_i) |u_{jo} - u_o| \qquad (4)$$

where K_v is the (experimentally) determined velocity mixing coefficient

$r_{0.5}$ is the radial distance at which the local velocity is the mean of the core and free-stream velocities [i.e., $u_{0.5} = (u_{jo} + u_o)/2$]

r_i is the radius of the "potential core", the inner edge of the mixing layer.

Typically, K_v is correlated against the Mach number corresponding to $u_{0.5}$. According to Smoot[6]

$$K_v \simeq .047 \text{ for } 0 < M_{0.5} < 0.2$$

$$\simeq .028 \text{ for } 0.7 < M_{0.5} < 1.3$$

So there should be no major difference between low-speed data and transonic entrainment. Then, following Albertson, et al.[7] and Kuchemann and Weber,[3] the entrainment ratio n is given by

---

* The Taylor mixing theory gives the same form; Von Karman's somewhat different. The differences are not important here.

$$n = \frac{\text{free air entrained}}{\text{initial jet volume flow}} = k(x_j/r_j)(1 - u_o/u_{jo}) \qquad (5)$$

($k \approx 0.0415$ at low Mach numbers, according to Albertson et al.[7])

This relationship is applicable to that part of the jet close to the nozzle, the so-called "zone of establishment" where it still has a "potential core" of velocity u_{jo}. This limitation will be justified below.

It follows from equation (5) that the corresponding axial sink line of strength $q(x_j)$ per unit length is

$$q(x_j) = -\pi k r_j (u_{jo} - u_o) \qquad (ft^3/sec.ft.)$$

the minus sign reminding us that it is a sink rather than a source line.

From Appendix A, the velocities induced at a point (x,r) by a constant strength sink in the region $0 < x_1 < \infty$ are

$$\Delta u = \frac{q(x_1)}{4\pi} \int_o^\infty \frac{(x - x_1)\, dx_1}{\left[(x - x_1)^2 + (\beta r)^2\right]^{3/2}} \qquad (6)$$

$$\Delta v = \frac{q(x_1)}{4\pi} \int_o^\infty \frac{\beta r^2\, dx_1}{\left[(x - x_1)^2 + (\beta r)^2\right]^{3/2}} \qquad (7)$$

Figure 6 shows that most of the effect on Δu is due to the first five diameters or so of the jet, thus justifying our neglect of the far-jet entrainment functions. [The "zone of establishment" typically has a length of roughly $9r_j/\lambda$, where $\lambda = (u_j/u_o - 1)$]. With $q(x_1)$ a constant, equations (6) and (7) may be immediately integrated to give

$$\Delta u = \frac{q(x_1)}{4\pi} \left[\frac{1}{\sqrt{(x - x_1)^2 + (\beta r)^2}} - \frac{1}{\sqrt{x^2 + (\beta r)^2}} \right]$$

$$= -\frac{q(x_1)}{4\pi} \frac{1}{\sqrt{x^2 + (\beta r)^2}} \quad \text{as } x_1 \to \infty \qquad (8)$$

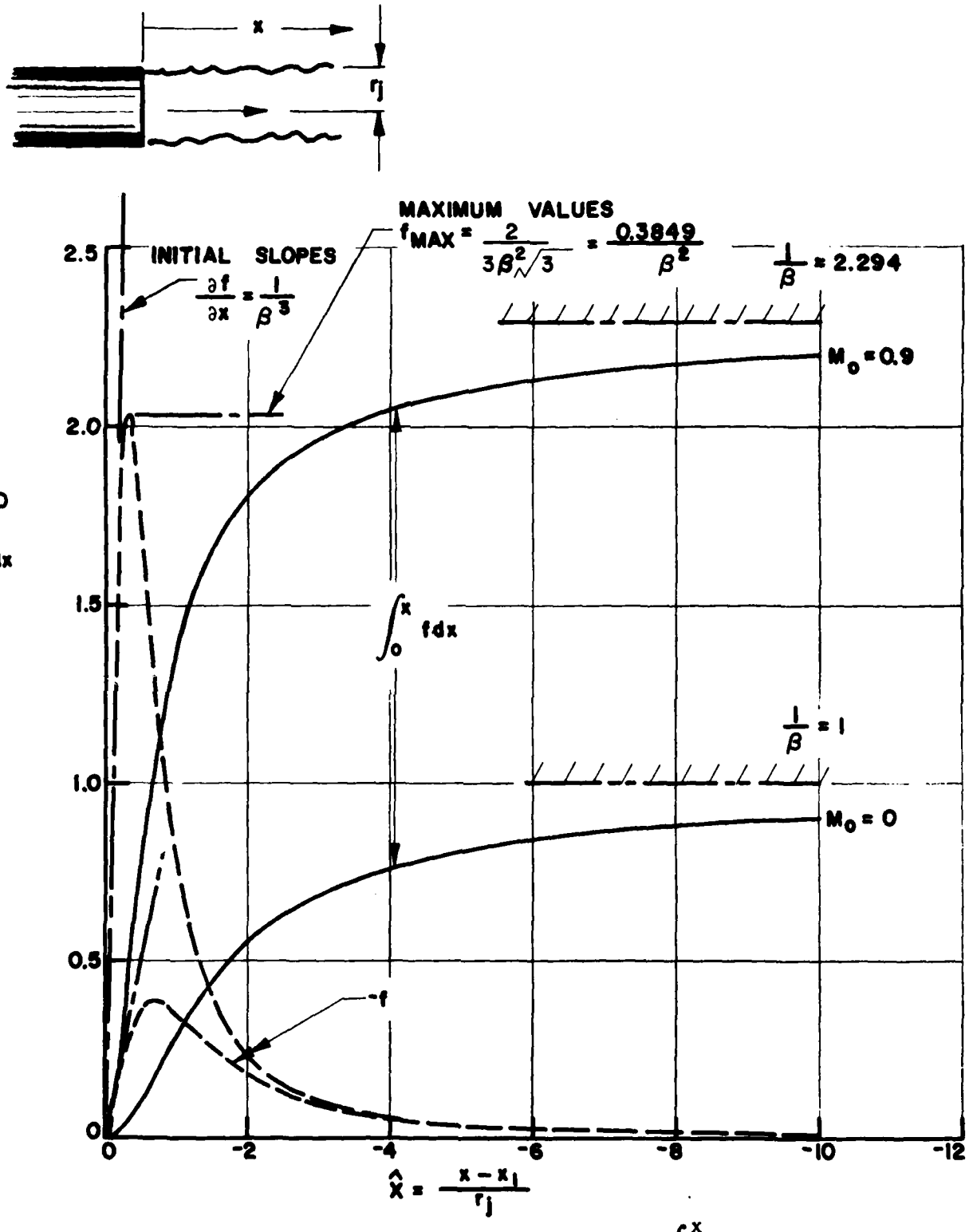

Figure 6. The Functions $f = \frac{x}{[x^2 + \beta^2\hat{r}^2]^{3/2}}$ and $\int_o^x f\,dx$ for Mach Numbers $M_o = 0$ and 0.9, $\hat{r} = \frac{r}{r_j} = 1$ and $\beta = \sqrt{1 - M^2}$.

$$\Delta v = -\frac{q(x_1)}{4\pi r}\left[\frac{(x - x_1)}{\sqrt{(x - x_1)^2 + (\beta r)^2}} - \frac{x}{\sqrt{x^2 + (\beta r)^2}}\right]$$

$$= \frac{q(x_1)}{4\pi r}\left[\frac{x}{\sqrt{x^2 + (\beta r)^2}} + 1\right] \quad \text{as } x_1 \to \infty \tag{9}$$

Making the substitution for $q(x_1)$:

$$\Delta u = \frac{kr_j}{4}\frac{(u_{jo} - u_o)}{\sqrt{x^2 + (\beta r)^2}} \tag{10}$$

$$\Delta v = -\frac{k}{4}\left(\frac{r_j}{r}\right)(u_{jo} - u_o)\left[\frac{x}{\sqrt{x^2 + (\beta r)^2}} + 1\right] \tag{11}$$

These are plotted in Figure 7. It's clear that as $x_j \to -\infty$, $\Delta u \to 0$. As $x_j \to \infty$, $\Delta u \to 0$ but

$$\Delta v \to (k/2)(r_j/r)(u_{jo} - u_o)$$

which is simply the flow into a two-dimensional sink, of strength $\pi k r_j (u_{jo} - u_o)$. It's also clear since $k = 0(10^{-1})$ that

$$\frac{\Delta u}{u_o} >> \left(\frac{\Delta u}{u_o}\right)^2$$

$$>> \left(\frac{\Delta v}{u_o}\right)^2$$

Thus, from equation A16 of Appendix A:

$$\Delta C_{P_{\beta E}} = -2\frac{\Delta u}{u_o} = -\frac{\frac{k}{2}\left(\frac{u_{jo}}{u_o} - 1\right)}{\sqrt{\hat{x}^2 + \beta^2\hat{r}^2}} = \frac{-\mu}{\sqrt{\hat{x}^2 + \beta^2\hat{r}^2}} \tag{12}$$

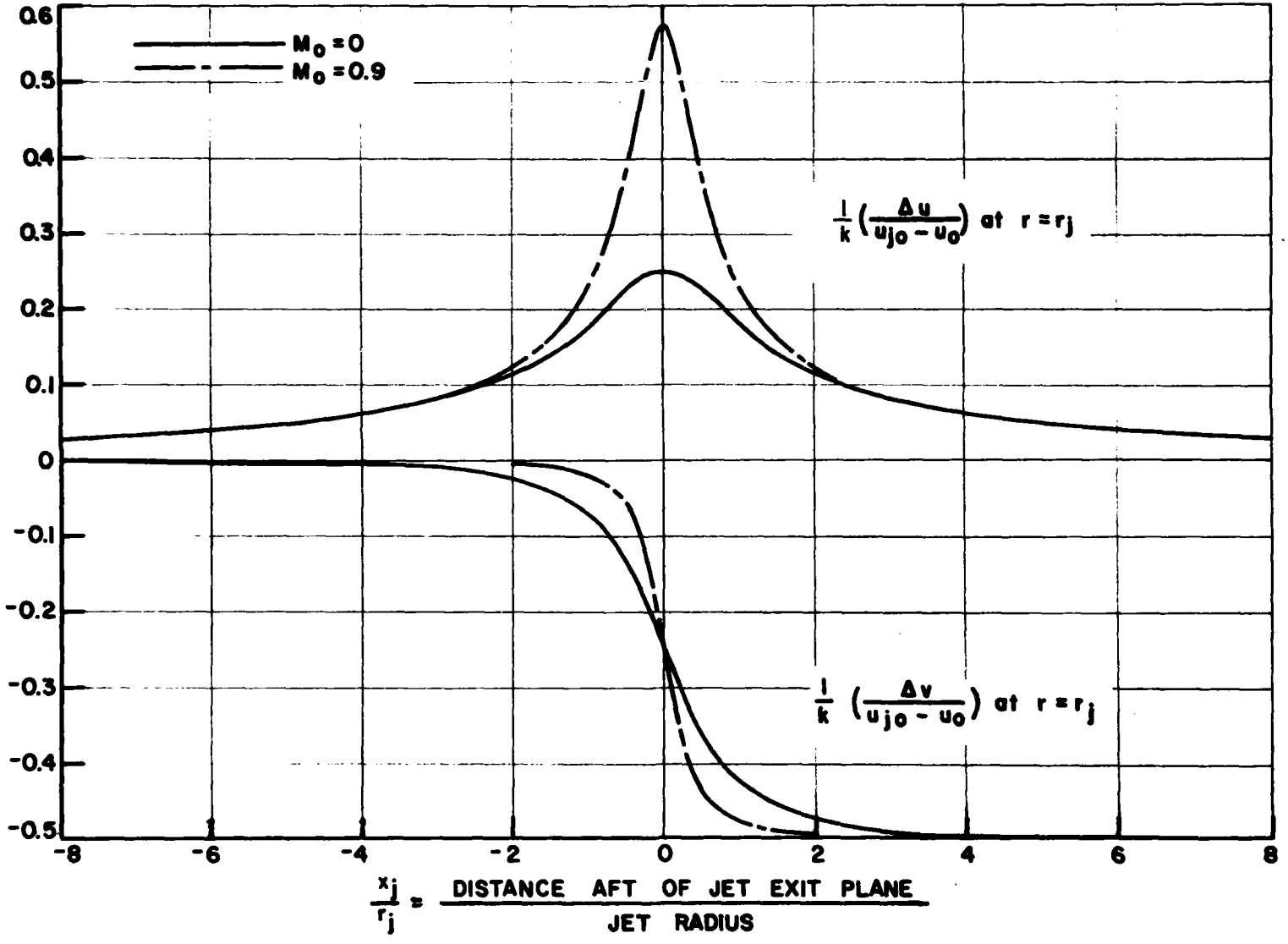

Figure 7. The Longitudinal and Radial Velocity Perturbation Components due to the Uniform Jet Entrainment Sink Model.

where $\hat{x} = x/r_j \qquad \hat{r} = r/r_j$

$$\mu = (k/2)(u_{jo}/u_o - 1) \approx \frac{k\lambda}{2}$$

A simple numerical example of equation (12) is given in Figure 8 for a cylindrical afterbody, $r_m = r_j$. The value of $C_{P_{\beta E}}$ will be smaller when $r_m > r_j$, of course.

It's now possible to integrate equation (12) over an afterbody in order to determine $C_{D_{\beta E}}$.

One convenient representation for an afterbody is a polynomial

$$r = r_j(1 + Az + Bz^2 + \ldots) \tag{13}$$

where $z = -x_j$, the longitudinal ordinate measured forward from the jet exit plane. An element of surface is $2\pi r\, ds$ and the projected area $2\pi r(dr/dz)dz$. Thus, the drag change is

$$d(\Delta D_E) = -\frac{1}{2}\rho u_o^2 \, \Delta C_{P_{\beta E}} \, 2\pi r \, \frac{dr}{dz} \, dz$$

$$\frac{d}{dz}(\Delta C_{D_{\beta E}}) = \frac{-2\Delta C_{P_{\beta E}}}{r_m^2} \, r \, \frac{dr}{dz}$$

Substituting for ΔC_P from equation (12)

$$\frac{d}{dz}(\Delta C_{D_{\beta E}}) = \frac{2\mu r \, dr/dz}{r_m^2 \sqrt{z^2 + \beta^2 \hat{r}^2}}$$

$$\therefore \frac{\Delta C_{D_{\beta E}}}{\mu} = \frac{2}{\hat{r}_m^2} \int_o^{z_m} \frac{(1 + Az + Bz^2 + \ldots)(A + 2Bz + \ldots)\, dz}{\sqrt{z^2 + \beta^2 (1 + Az + Bz^2 + ..)^2}} \tag{14}$$

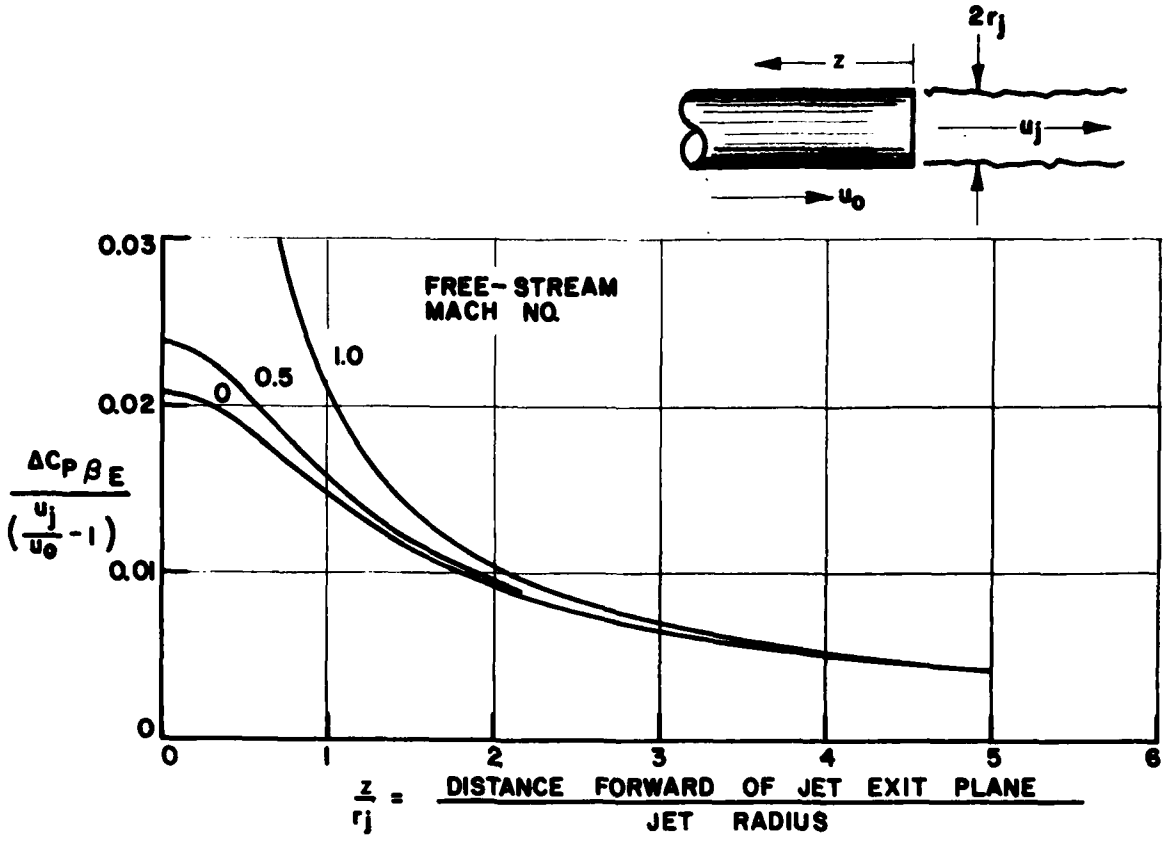

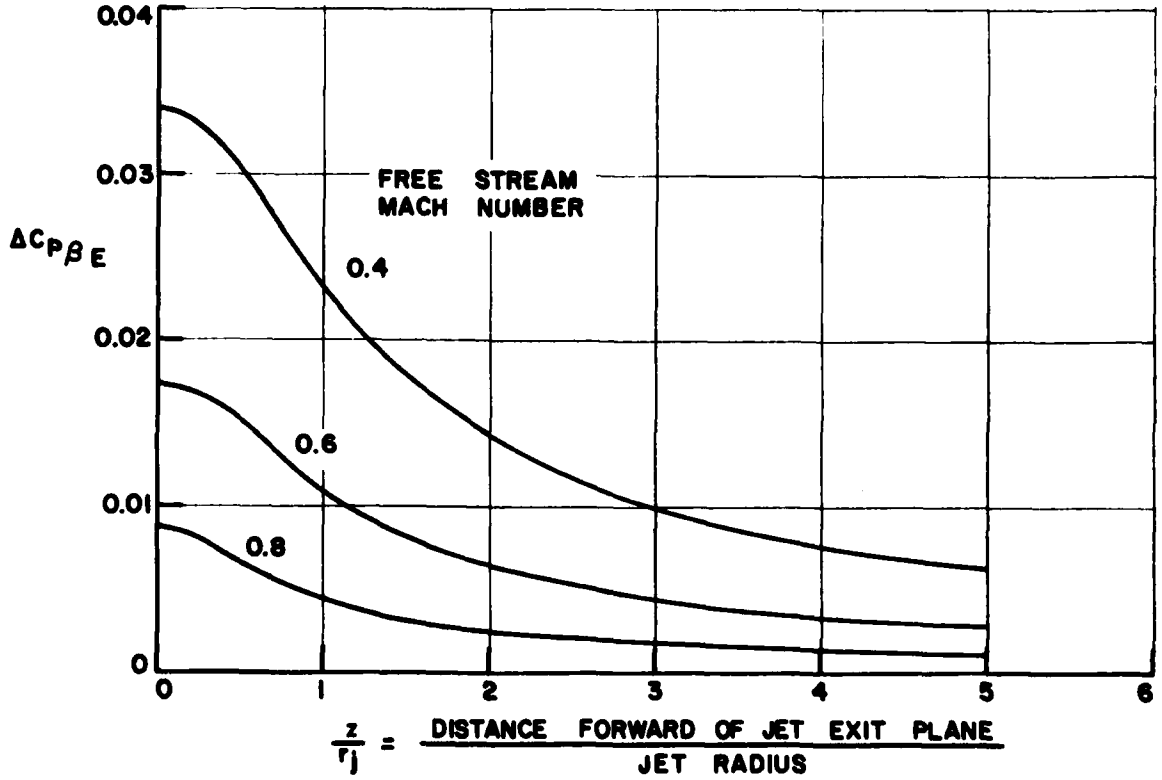

Figure 8. The Effect of Free-Stream Mach Number on the Entrainment Suction Distribution; Constant Jet Velocity of Unity Mach Number.

which can be numerically integrated for any number of terms. For the simplest case of a conical afterbody:

$$\frac{\Delta C_{D_{\beta E}}}{\mu} = \frac{2A}{\hat{r}_m^2} \int_0^{z_m} \frac{(1 + Az)dz}{\sqrt{(1 + \beta^2 A^2)z^2 + 2A\beta^2 z + \beta^2}} \qquad (15)$$

where A = tan θ, the tangent of the cone half angle.

This is conveniently written in terms of

$$\psi = \beta A, \quad z = \frac{\hat{r} - 1}{A}, \quad \frac{dz}{d\hat{r}} = \frac{1}{A}$$

Then

$$\frac{\beta \Delta C_{D_{\beta E}}}{\mu} = \frac{2\psi}{\hat{r}_m^2} \int_1^{\hat{r}_m} \frac{\hat{r}\, d\hat{r}}{\sqrt{(1 + \psi^2)\hat{r}^2 - 2\hat{r} + 1}}$$

$$= \frac{2\psi}{\hat{r}_m^2} \left\{ \frac{1}{(1 + \psi^2)} \left[\sqrt{(1 + \psi^2)\hat{r}_m^2 - 2\hat{r}_m + 1} - \psi \right] \right.$$

$$\left. + \frac{1}{(1 + \psi^2)^{3/2}} \left[\sinh^{-1}\left(\frac{(1 + \psi^2)\hat{r}_m - 1}{\psi} \right) - \sinh^{-1}(\psi) \right] \right\} \qquad (16)$$

This equation is plotted in Figure 9, which gives $\Delta C_{D_{\beta E}}$ for any combination of $\hat{r}_m$, θ and M. Some specific values are given in Figure 10. Note that the "shape factor" $\Phi = \Delta C_{D_{\beta E}}/\mu$ is a function only of afterbody shape and freestream Mach number. Theoretical values of $\Delta C_{D_{\beta E}}$ for a particular conical afterbody are plotted in Figure 11 for three different NPR's. It seems clear that the entrainment drag coefficient is less important at transonic speeds.

Using the approach described, it's obviously possible to express $\Delta C_{D_{\beta E}}$ for any afterbody as

$$\Delta C_{D_{\beta E}} = (k/2)(u_{jo}/u_o - 1)\Phi \qquad (17)$$

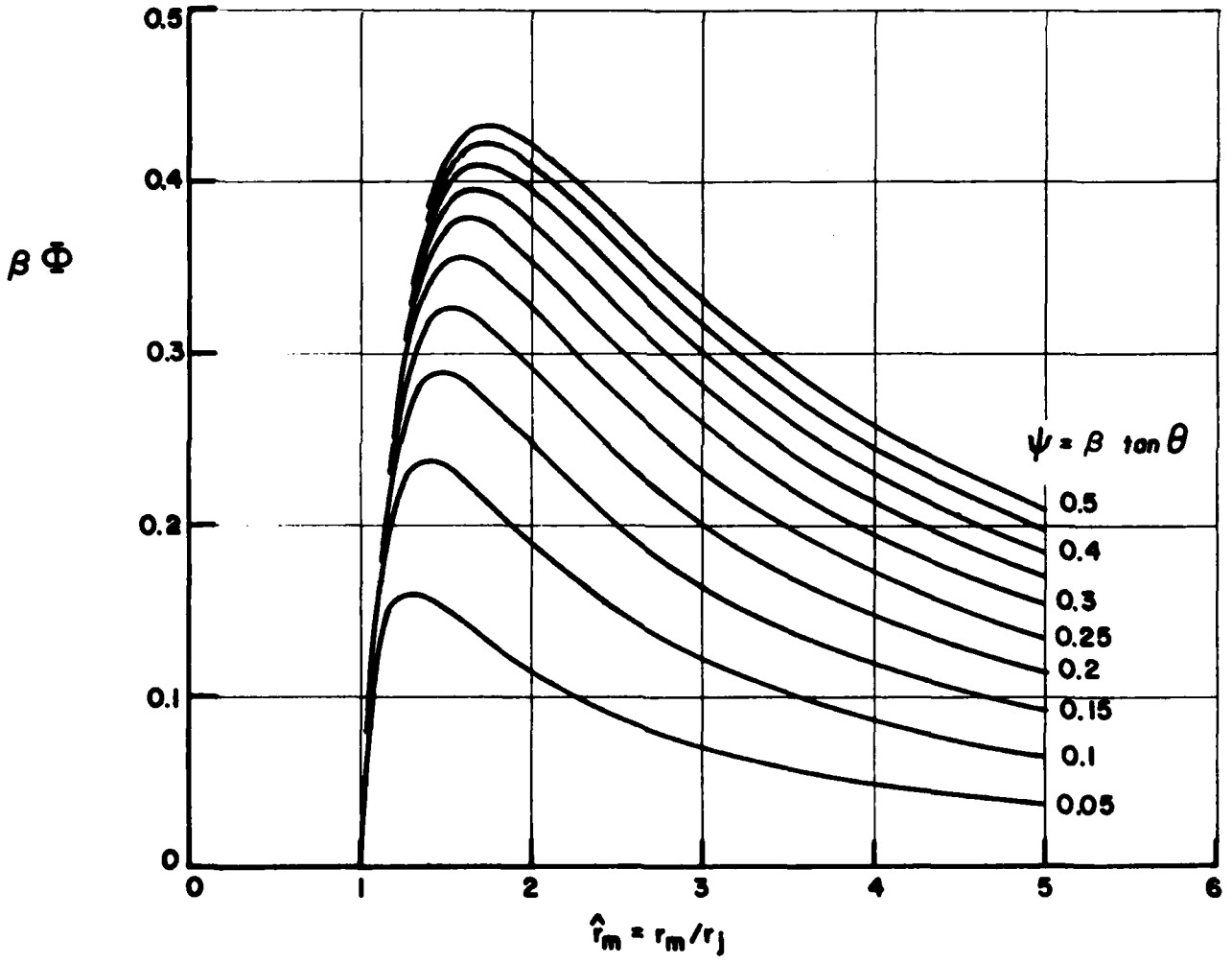

Figure 9. Generalized Plot of the Entrainment Parameter Φ for Conical Afterbodies.

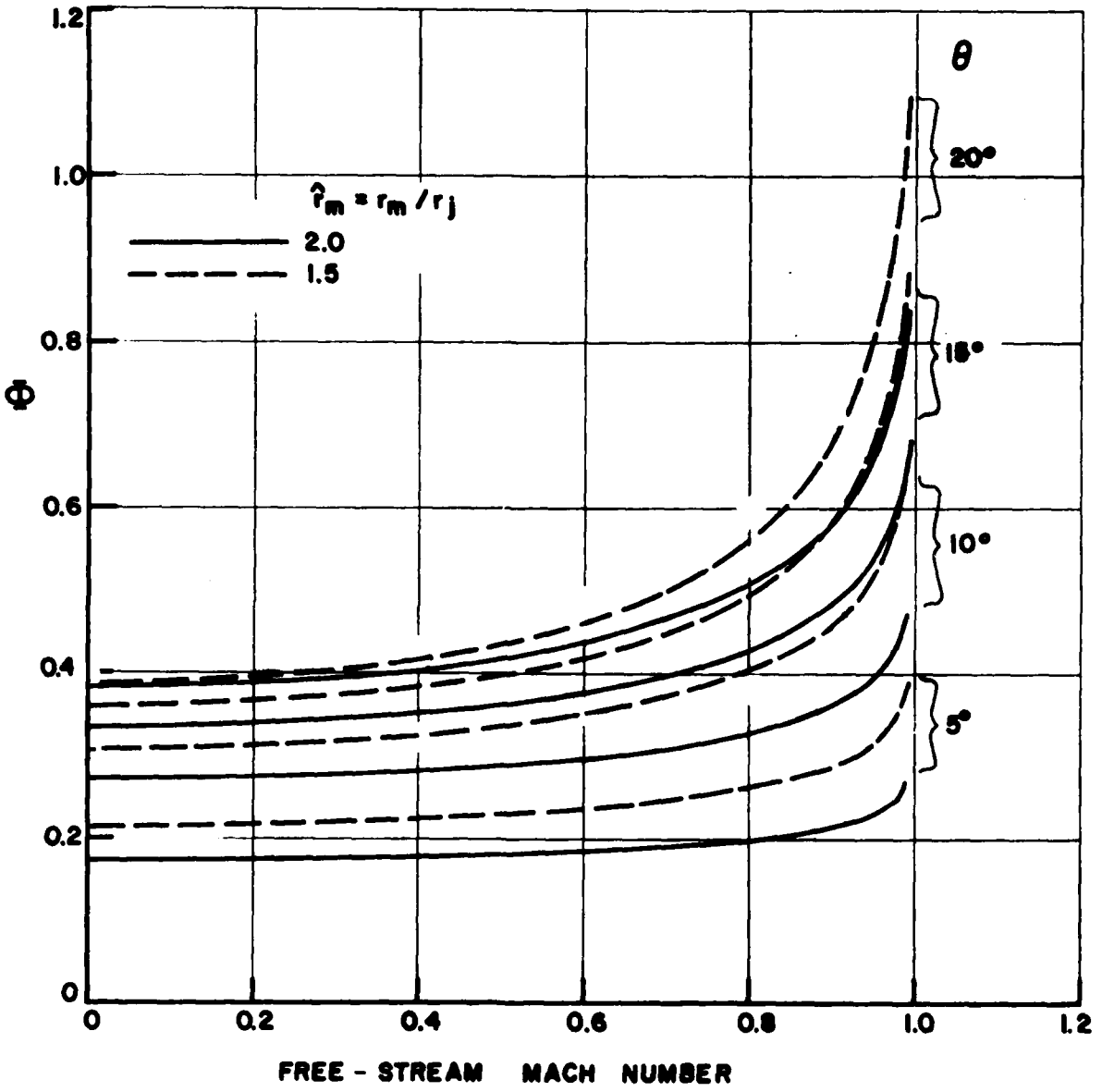

Figure 10. The Shape Factor Φ for Some Representative Conical Afterbody Shapes, as a Function of Mach Number.

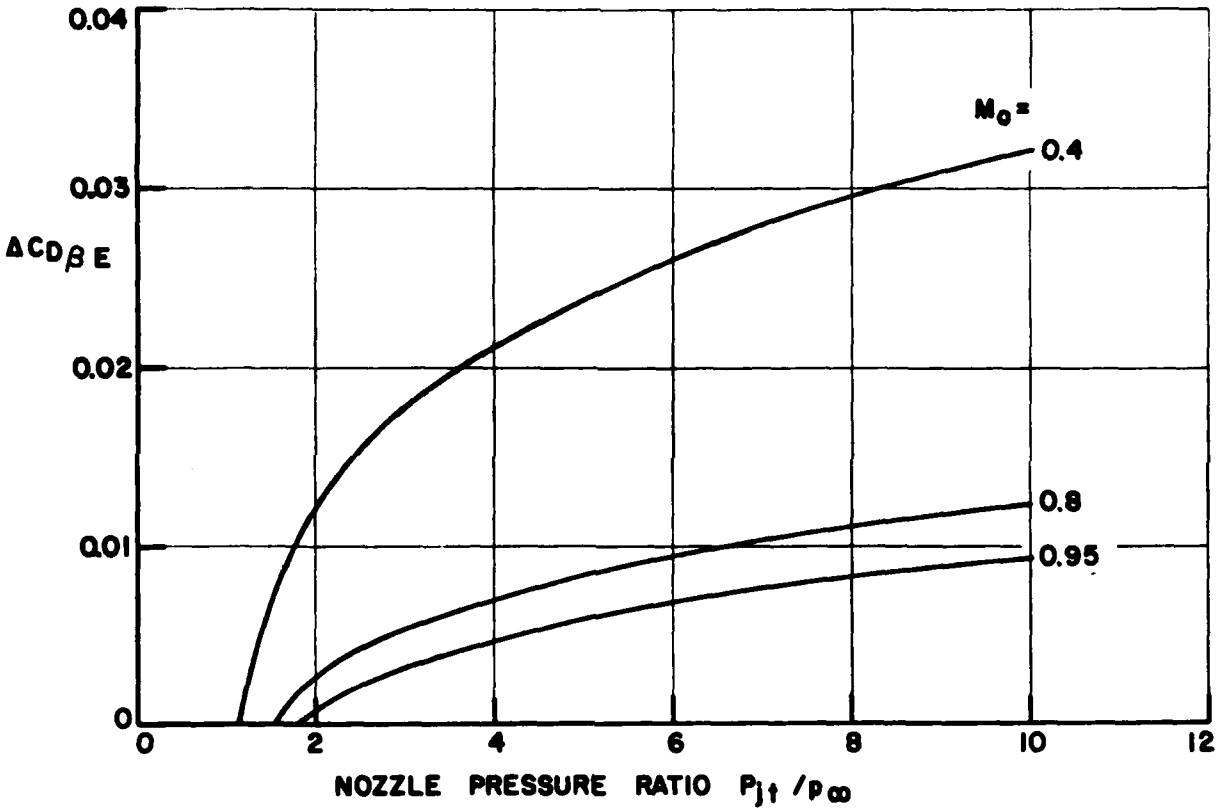

Figure 11. Theoretical Entrainment Drag Increment for a Conical Nozzle Having a 15° Half Angle. $\hat{r}_m = 2.0$, $k = .0415$

where the shape factor Φ is given by

$$\Phi = \frac{2}{\hat{r}_m^2} \int_0^{z_m} \frac{\hat{r}(d\hat{r}/dz)dz}{\sqrt{z^2 + \beta^2 \hat{r}^2}} = \frac{2}{\hat{r}_m^2} \int_1^{\hat{r}_m} \frac{\hat{r}\, d\hat{r}}{\sqrt{z^2 + \beta^2 \hat{r}^2}} \qquad (18)$$

Note that when $z^2 << \beta^2 \hat{r}^2$

$$\Phi \rightarrow \frac{2}{\beta \hat{r}_m^2} (\hat{r} - 1) \qquad (19)$$

Equation (17) now explains some previously puzzling phenomena and enables us (in principle) to better reduce experimental data to a common denominator. Figure 12 shows some of the Reubush[8] data plotted against $(M_j/M_o - 1)$, which we have assumed to be the same as $(u_{jo}/u_o - 1)$, since the jet was "cold." The raw data of reference 8 shows that, for a given NPR, $C_{D\beta}$ reduces with increasing Mach number; an anomalous result. But when plotted as shown in Figure 12, we see that this is explained by the reduction of $\Delta C_{D_{\beta E}}$ with increasing Mach number, and that $C_{D_{\beta 0}}$, the value for zero entrainment, (given by the intercepts in Figure 12) increases with Mach number as we would expect.

Figure 13 gives a more detailed plot of $C_{D_{\beta 0}}$, for another circular arc nozzle, which was obtained in the same way. Most unfortunately, there is very little data available in the literature for subsonic jet velocities, so that it is not possible to produce parametric curves of $C_{D_{\beta 0}}$, as has been done for the jet-off case. $C_{D_{\beta 0}}$ for some NASA circular arc boattails is plotted in Figure 14, as a function of their equivalent cone angle, and considering the accuracy with which the raw data can be obtained from the original references and the extreme paucity of subsonic jet data points (usually two; never more than three), the scatter is considered to be reasonable. The basic data for these boattails is given in Table 1. The slope of the data in Figure 12 gives the value of the entrainment function k, since, from equation (17)

$$k = \frac{2\Delta C_{D_{\beta E}}}{\Phi(u_{jo}/u_o - 1)} \qquad (20)$$

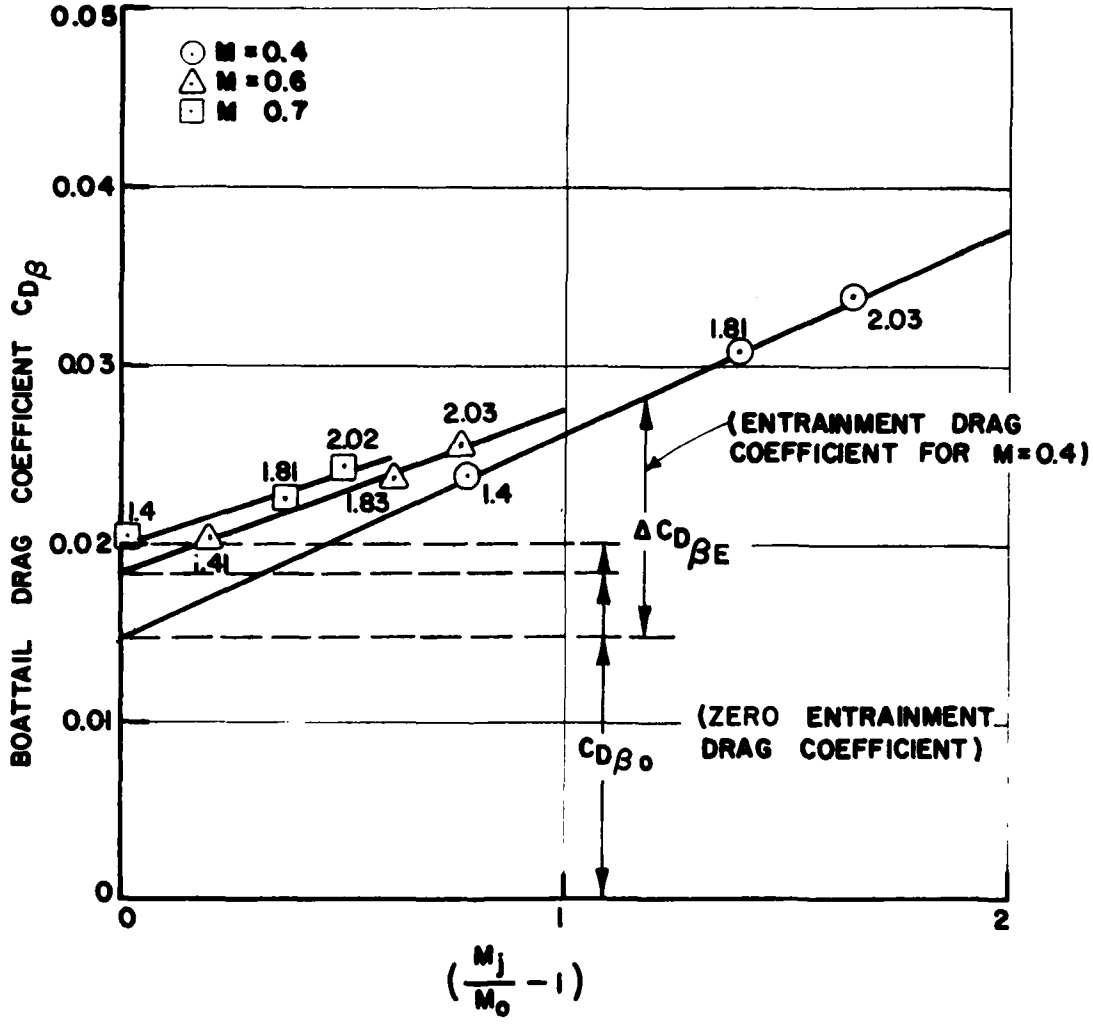

Figure 12. Variation of Boattail Drag with the Velocity Ratio Parameter, for a NASA Circular Arc Boattail. $D_E/D_M = 0.6$, $\ell/D_M = 1.0$. (The Small Numbers Give NPR for Each Data Point).

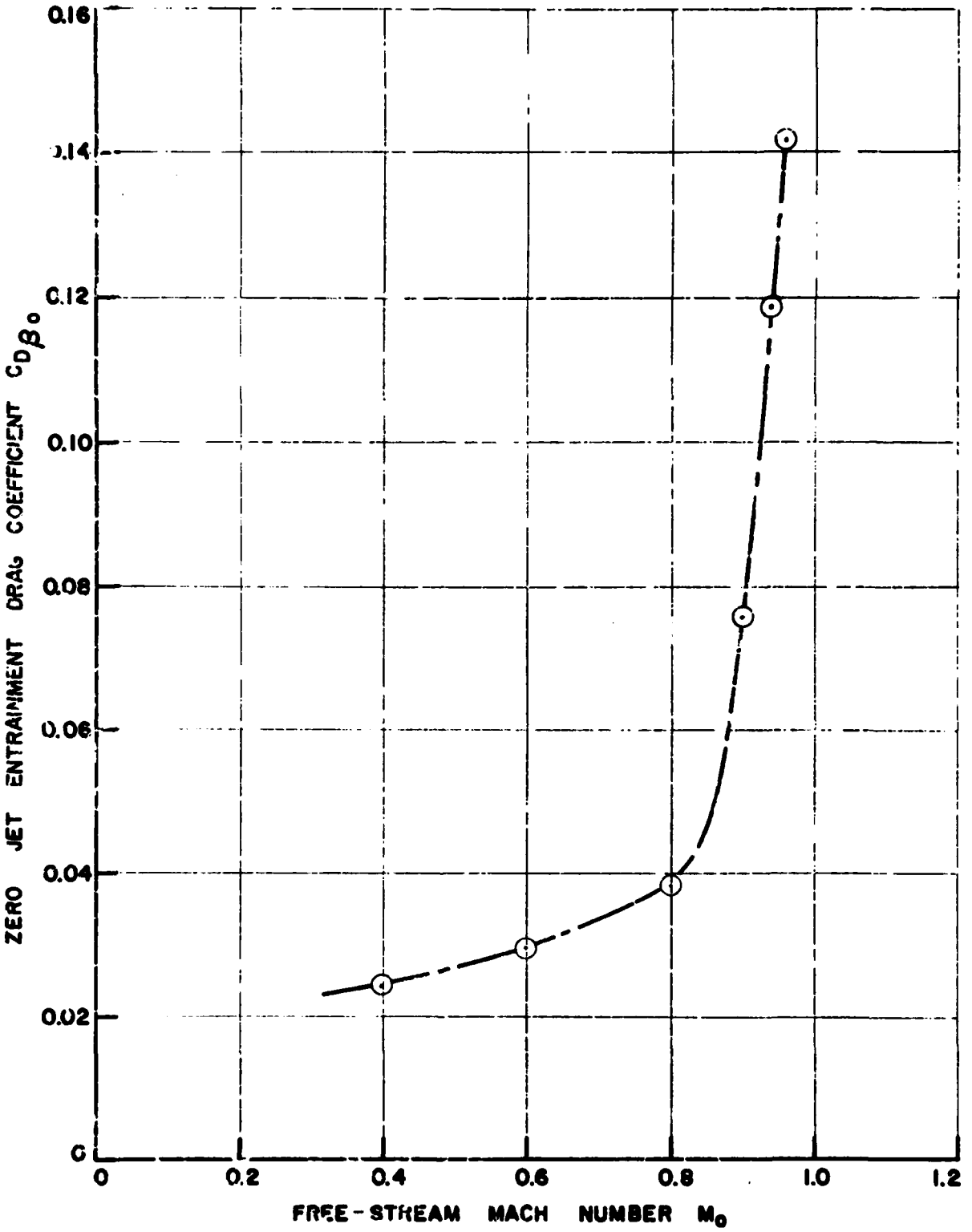

Figure 13. Zero Entrainment $C_{D_{\beta_0}}$ for a NASA Circular Arc Afterbody (NASA TN - D-7192), $D_E/D_M = 0.5$, $\ell/D_M = 0.8$.

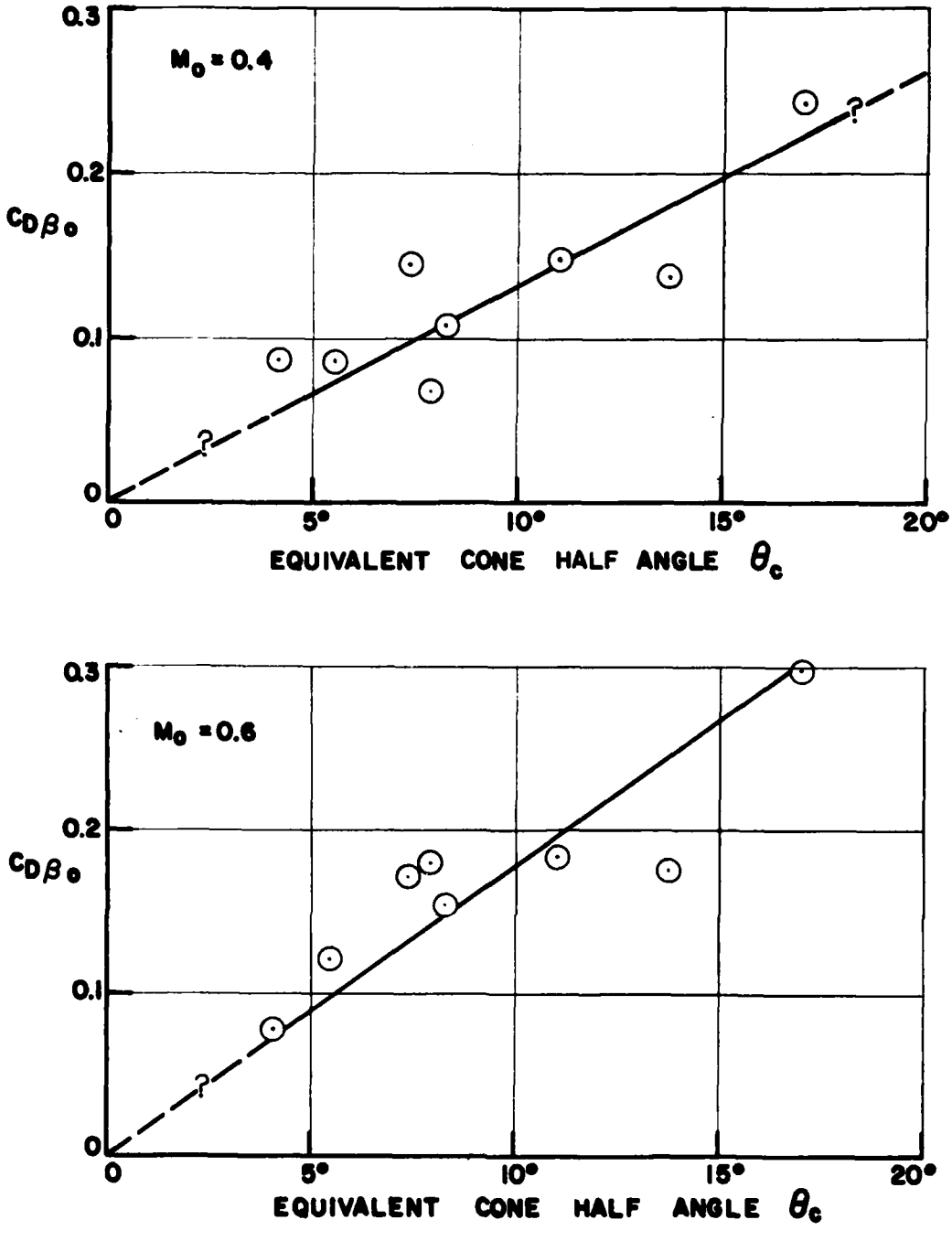

Figure 14. Zero Entrainment Drag of the NASA Circular Arc Boattails as a Function of Their Equivalent Cone Angle. (Data from References 8 and 11).

TABLE 1. DATA FOR NASA CIRCULAR ARC NOZZLES, FROM REFERENCES 8 AND 11.

$\frac{D_E}{D_M}$	$\frac{\ell}{D_M}$	M	Φ	$C_{D_{\beta 0}}$	$\frac{\Delta C_{D_{\beta E}}}{\left(\frac{u_j}{u_o} - 1\right)}$	k	θ_f	θ_c
0.6	1.0	0.4	0.404	.0147	.0114	.0564	22.07°	11.03°
		0.6	0.442	.0184	.0091	.0412		
		0.7	0.475	.02	.0081	.0341		
0.6	1.5	0.4	0.346	.0145	.0084	.0486	14.81°	7.41°
		0.6	0.373	.0171	.0044	.0236		
		0.7	0.396	.0186	.0019	.0096		
0.7	1.0	0.4	0.354	.0107	.0099	.0559	16.50°	8.25°
		0.6	0.388	.0153	.0048	.0247		
		0.7	0.417	.0167	.0018	.0086		
0.7	1.5	0.4	0.305	.0086	.0073	.0479	11.04°	5.52°
		0.6	0.330	.012	.0044	.0267		
		0.7	0.352	.014	-	-		
0.7	2.0	0.4	0.269	.0086	.0054	.0401	8.29°	4.15°
		0.6	0.288	.0077	.0027	.0188		
		0.7	0.305	.0084	.0014	.0092		
0.5	0.8	0.4	0.45	.0243	.0167	.0742	34.04°	17.02°
		0.6	0.496	.0296	.0154	.0621		
		0.8	0.599	.0382	.0168	.0561		
0.5	1.0	0.4	0.419	.0137	.013	.0621	27.52°	13.76°
		0.6	0.458	.0175	.0103	.0450		
0.5	1.768	0.4	0.328	.0068	.0087	.0530	15.77°	7.89°
		0.6	0.351	.018	.0057	.0325		

Average k = .0548 for M = 0.4
= .0343 for M = 0.6
= .0154 for M = 0.7

The shape factor Φ, obtained by numerical integration of equation (18), is given in Figure 15, and the derived values of k in Figure 16. It's encouraging to note that k is of the right order and that it falls with increasing Mach number. The increase of k with the equivalent cone half-angle is presumably due to the nonlinear boundary effects mentioned at the beginning of this discussion. A more refined analysis would recognize that $u < u_o$ in the boundary layer leads to higher entrainment rates and that the thicker the boundary layer (i.e., the greater the equivalent half angle), the more important this effect would be. A more refined analysis would also compute the important change in the boundary layer displacement thickness with increasing entrainment.

NSRDC boattail 10 has no base area and so can be compared with the theory as shown in Figure 17. The value of $k = 0.02$ was extrapolated from Figure 16, which clearly needs to be expanded. The value of Φ was read from Figure 9, even though boattail 10 is not a simple cone, because the fairing into the body is furthest removed from the jet, and the error should therefore be tolerable.

PLUME INTERFERENCE

As indicated in Figure 18, plume interference is characterized by an increase in static pressure on the boattail. If the jet diameter is smaller than the base, the length of the separation streamline tends to partially insulate the boattail. Thus, when there is a substantial base area "insulating" the boattail from the jet, the plume effect on boattail drag can be negligible for moderate values of NPR.

The first step in understanding the phenomena is to estimate the shape of the plume. To do this, we first determine the initial turning angle δ_j, defined in Figure 19.

It's been observed by many workers that the initial jet turning angle δ_j is not much affected by the free stream flow conditions, so that

$$\delta_j \simeq \nu_1 - \nu_N + \alpha_N \qquad (21)$$

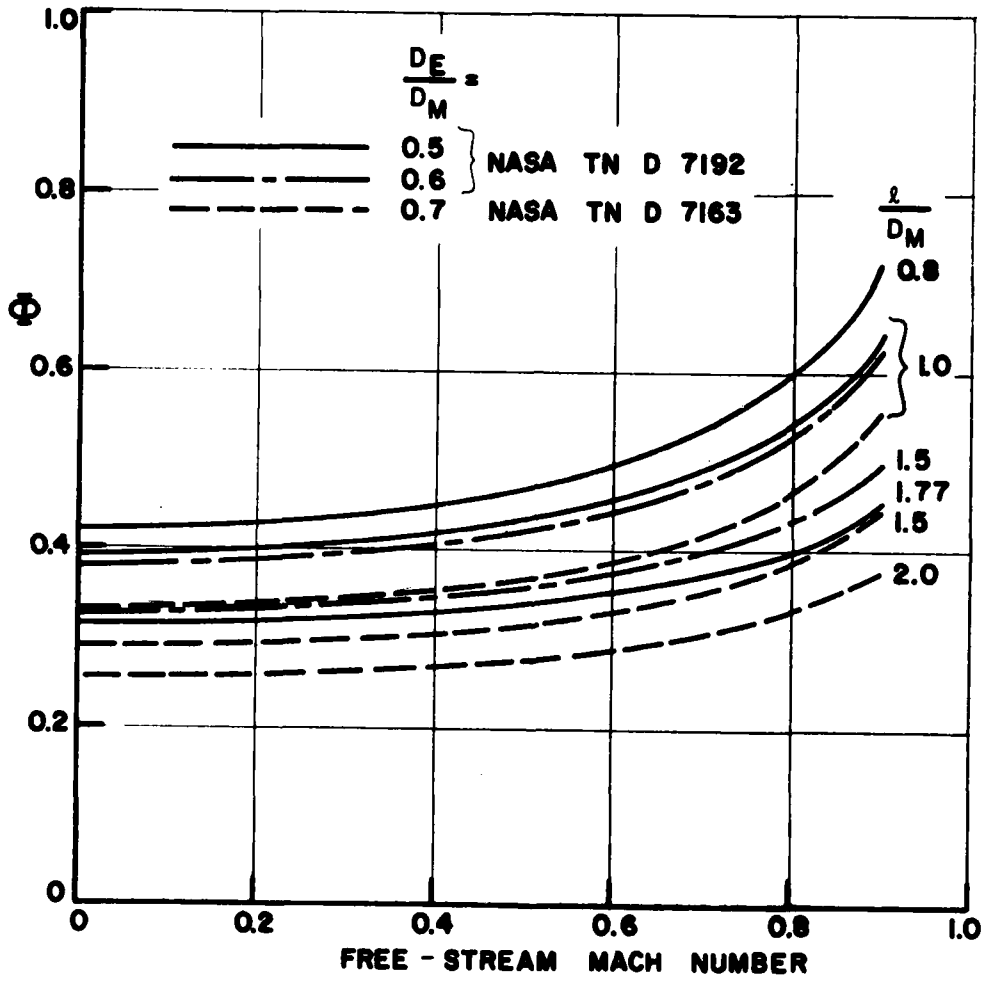

Figure 15. The Shape Factor Φ for Some NASA Circular Arc Boattails.

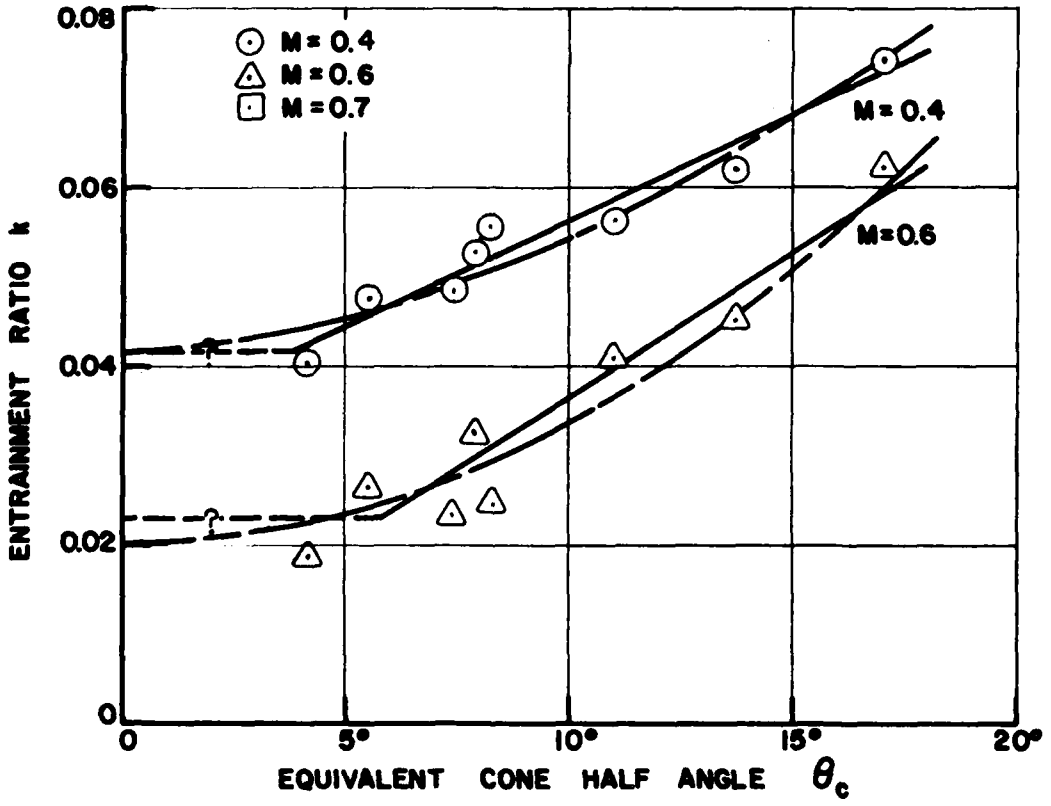

Figure 16. Variation of Entrainment Ratio k with Free-Stream Mach Number and Equivalent Cone Angle for the NASA Circular Arc Nozzles. (The precise form of the variation is not known at the present time.)

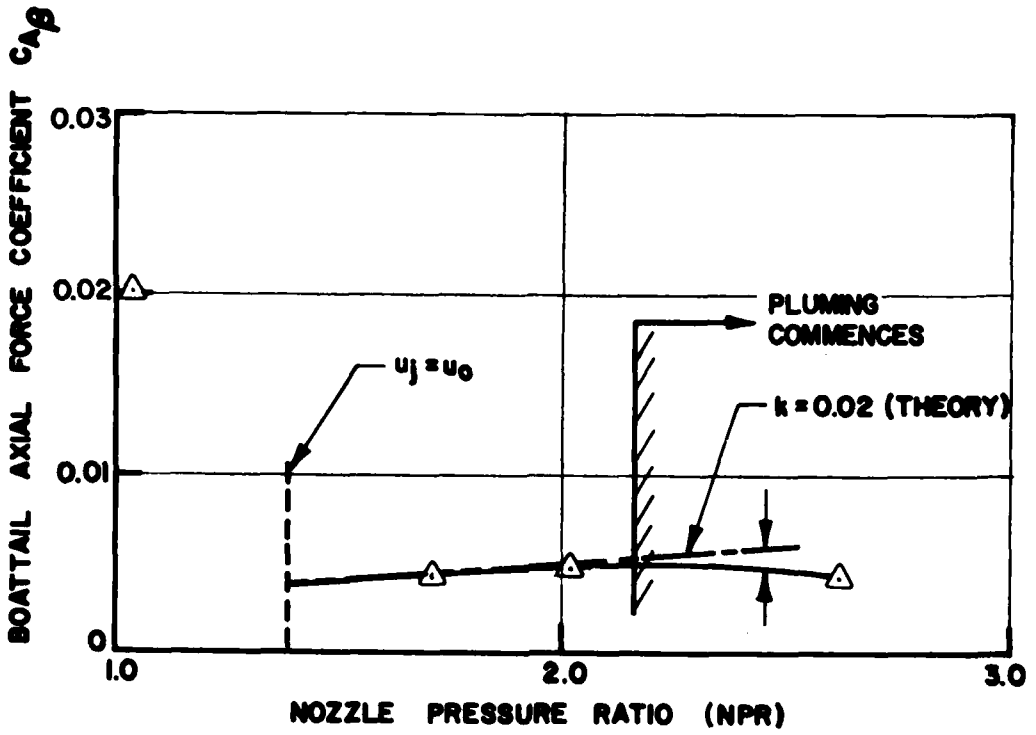

Figure 17. A Comparison Between Entrainment Theory and DTNSRDC Measurements on Body 70010 at M = 0.7.

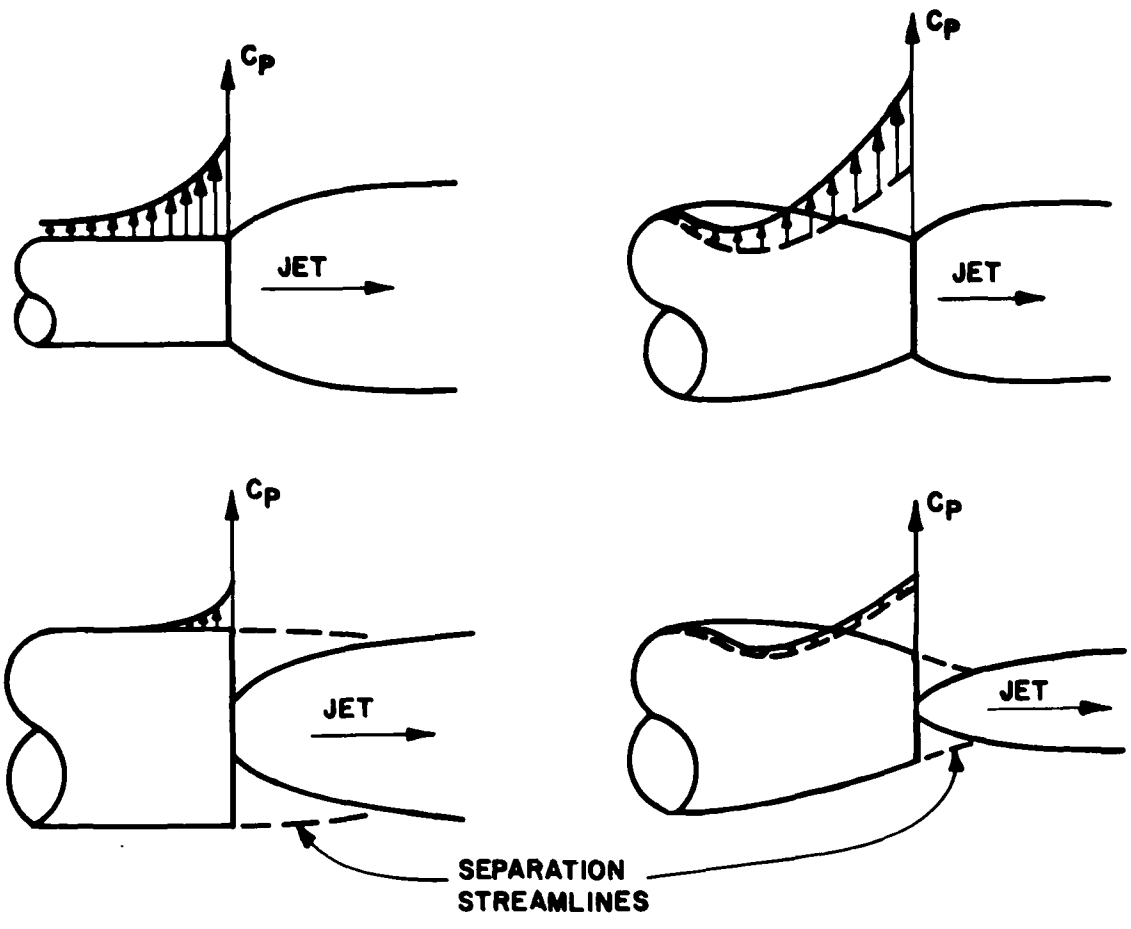

Figure 18. The Magnitude of Plume Interference on the Boattail Depends on the Ratio of Jet to Base Diameters.

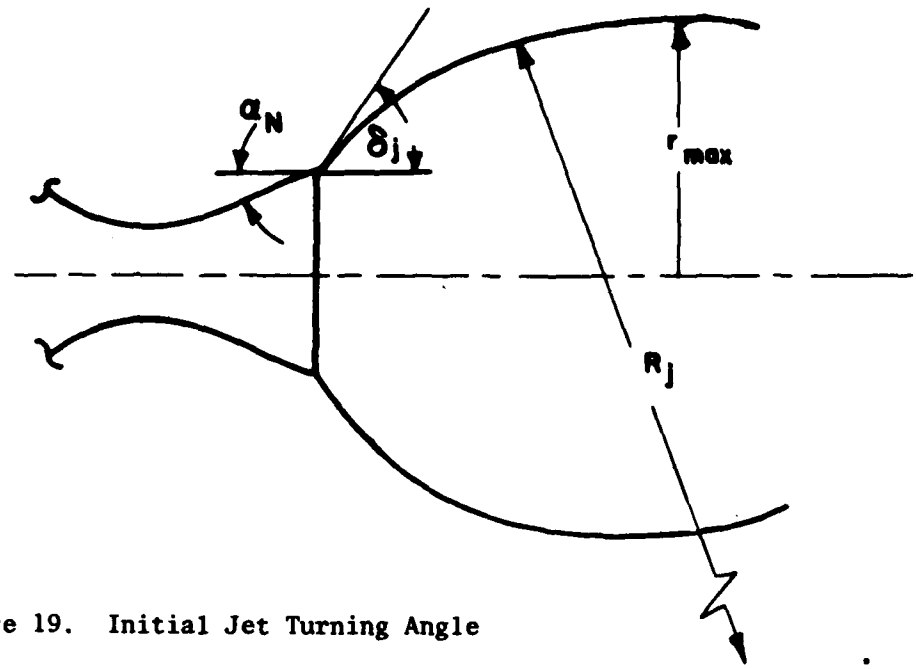

Figure 19. Initial Jet Turning Angle

where υ_1 = the Prandtl-Meyer expansion angle for the plume boundary Mach number M_B

$$= \sqrt{\frac{\gamma + 1}{\gamma - 1}} \tan^{-1} \sqrt{\frac{\gamma - 1}{\gamma + 1} (M_B^2 - 1)} \quad -\tan^{-1} \sqrt{M_B^2 - 1} \qquad (22)$$

υ_N = the Prandtl-Meyer expansion angle for the nozzle exit Mach number M_N

$$= \sqrt{\frac{\gamma + 1}{\gamma - 1}} \tan^{-1} \sqrt{\frac{\gamma - 1}{\gamma + 1} (M_N^2 - 1)} \quad - \tan^{-1} \sqrt{M_N^2 - 1} \qquad (23)$$

where $M_B \simeq \sqrt{\left(\frac{2}{\gamma - 1}\right) \left[\left(\frac{p_{jt}}{p_\infty}\right)^{\frac{\gamma - 1}{\gamma}} - 1\right]}$ (24)

and M_N is specified by the nozzle design

If the flow were one-dimensional the maximum cross-sectional area (A_m) of the plume would be given by

$$A_{m1D} = \frac{A^*}{M_B}\left[\frac{2}{\gamma+1}\left(1+\frac{\gamma-1}{2}M_B^2\right)\right]^{\frac{\gamma+1}{2(\gamma-1)}}$$

$$= \frac{\left(\frac{2}{\gamma+1}\right)^{\frac{\gamma+1}{2(\gamma-1)}}\left(\frac{p_{jt}}{p_\infty}\right)^{\frac{\gamma+1}{2\gamma}}}{\sqrt{\frac{2}{\gamma-1}\left[\left(\frac{p_{jt}}{p_\infty}\right)^{\frac{\gamma-1}{\gamma}}-1\right]}} \qquad (25)$$

where A^* is the sonic throat area

Equation (25) is plotted in Figure 20 for typical pressure ratios. It turns out (as shown in Figure 21) that for zero nozzle angle the actual area ratio is quite precisely the square of this quantity, for NPR's less than about 20. A simple linear approximation is also shown in Figure 21.

In experimental measurements of plume boundaries, the static pressure p_E at the jet exit is often employed. This is related - again one dimensionally - to the jet exit Mach number M_E by

$$\frac{p_E}{p_{jt}} = \left(1+\frac{\gamma-1}{2}M_E^2\right)^{-\frac{\gamma}{\gamma-1}} \qquad (26)$$

$$\frac{p_E}{p_\infty} = \frac{p_E}{p_{jt}}\frac{p_{jt}}{p_\infty} = \frac{p_{jt}}{p_\infty}\left(1-\frac{\gamma-1}{2}M_E^2\right)^{-\frac{\gamma}{\gamma-1}} \qquad (27)$$

Underexpanded jet boundaries have been studied by many workers. Of particular note are the works by Love et al.[9] and Vick et al.,[10] both of which give additional important references. For the moderate nozzle

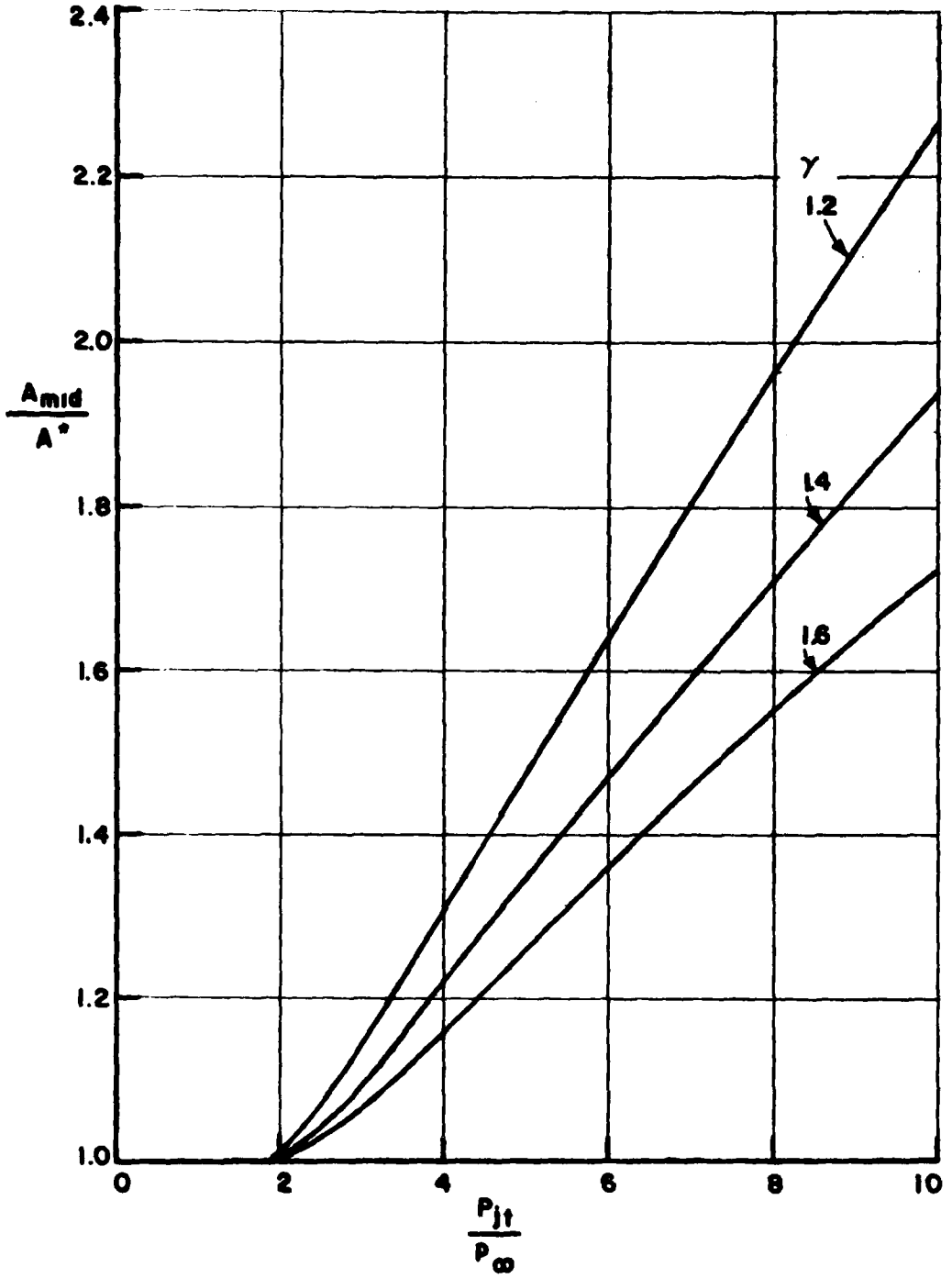

Figure 20. Maximum Plume Area from One-Dimensional Theory.

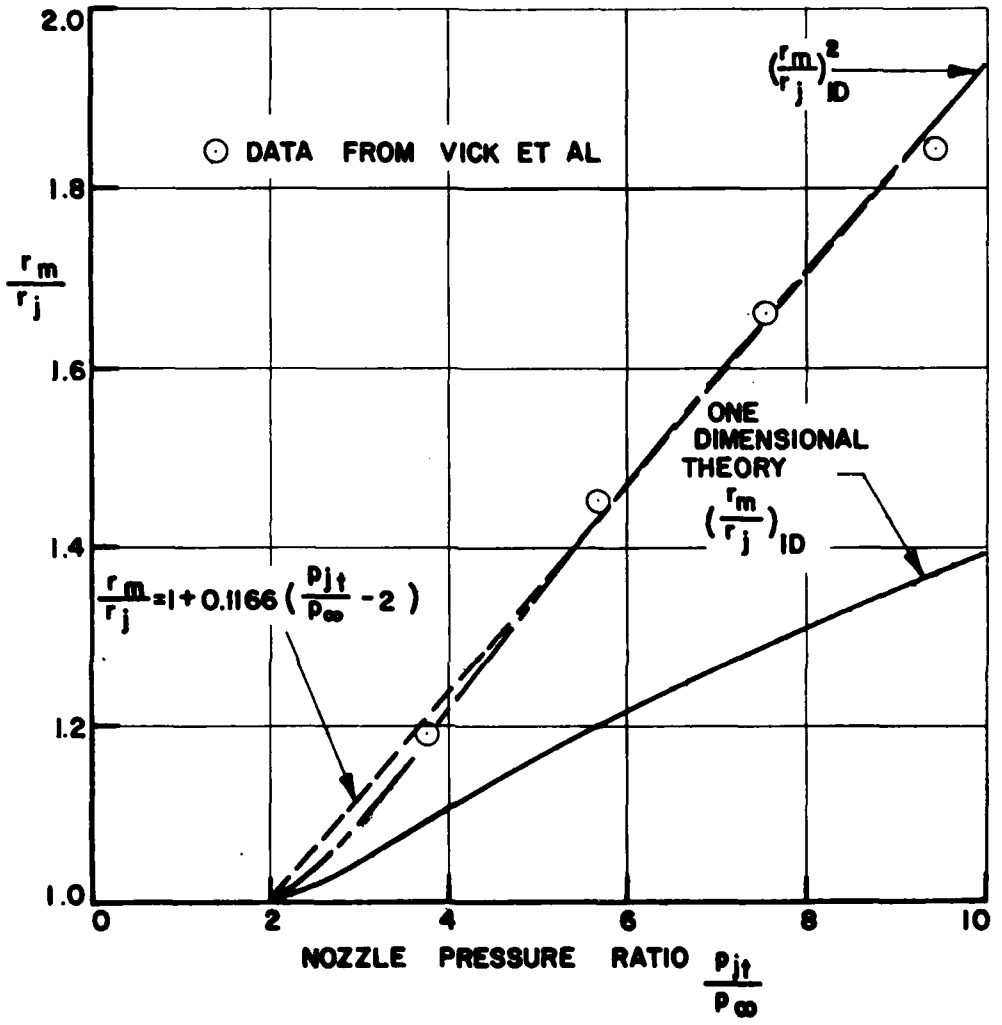

Figure 21. Maximum Plume Radius, as a Function of NPR for a Sonic Jet. (γ = 1.4)

pressure ratios of interest here it's generally concluded that the jet profile is adequately described by a circular arc between the nozzle exit and the maximum diameter, as indicated earlier in Figure 19. Unfortunately the equation for a circular arc is relatively complicated to integrate when using slender body theory. Accordingly, we here employ the second order polynominal

$$r = r_j + \delta_j x_j - \frac{\delta_j x_j^2}{2x_{jm}} \tag{28}$$

$$\text{where } x_{jm} = \frac{2(r_m - r_j)}{\delta_j}$$

For initial jet expansion angles of 0 - 30°, this gives a profile which is essentially identical with a circular arc.

From the theory of Appendix A we can now compute the velocity pertubations due to the plume and the resulting pressures on the boattail. From equation A.18

$$q(x_1) = 2\pi u_o r \frac{dr}{dx_j}$$

$$= 2\pi u_o \delta_j \left(r_j + \delta_j x_j - \frac{\delta_j x_j^2}{2 x_{jm}} \right) \left(1 - \frac{x_j}{x_{jm}} \right) \tag{29}$$

Some typical $q(x_j)$ variations are plotted in Figures 22 and 23. For small values of NPR

$$q(x_j) = 2\pi u_o r_j \delta_j (1 - \breve{x}_j) \qquad (\breve{x}_j = x_j/x_{jm}) \tag{30}$$

is not a bad approximation to equation (29). It becomes worse as NPR increases, but then, so does the slender body approximation itself. So although our discussion is initially more general, we shall return to this approximation for an engineering approximation to the plume effect.

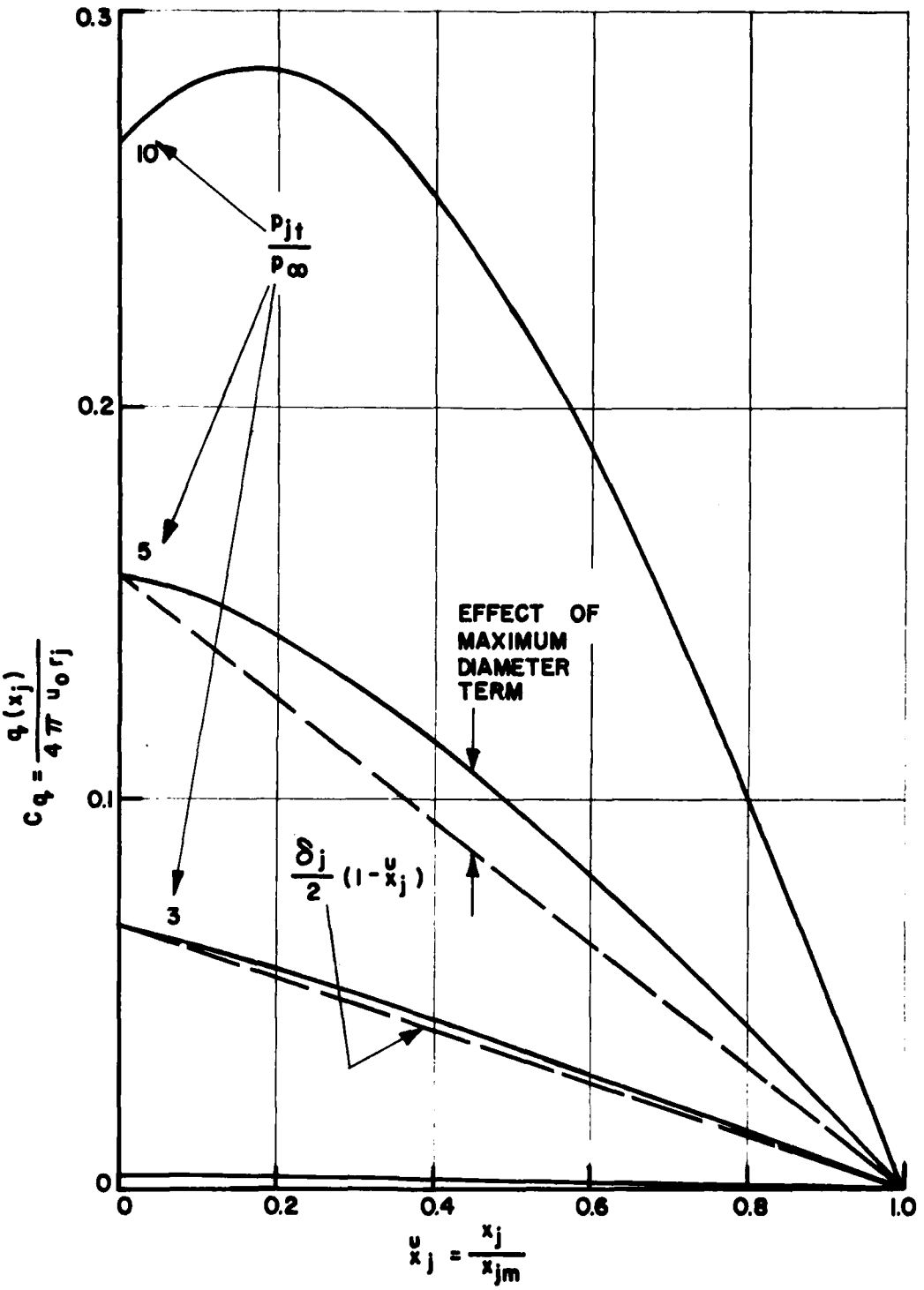

Figure 22. The Source Distribution Coefficient for Various Nozzle Pressure Ratios. Sonic Nozzle, $\gamma = 1.4$

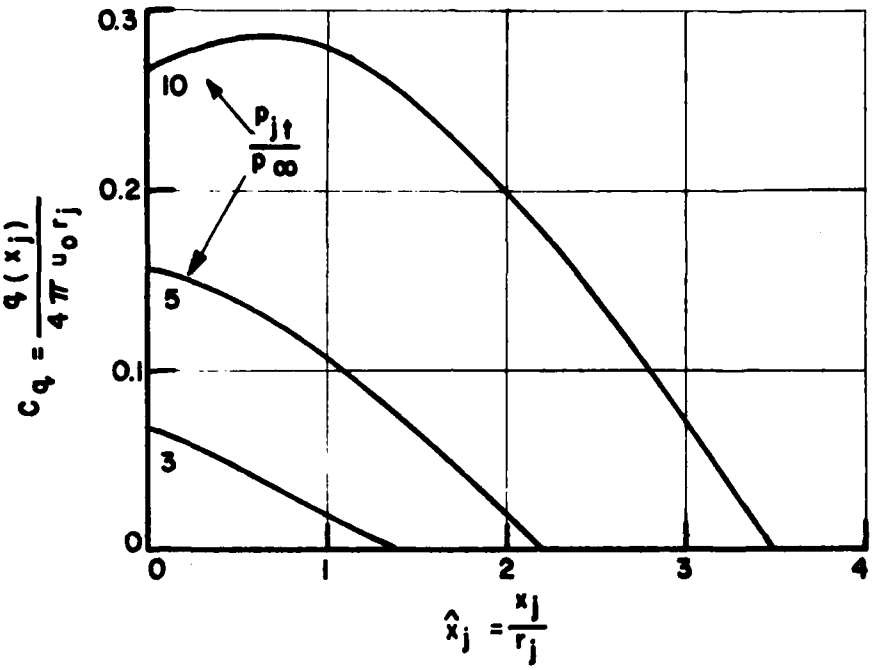

Figure 23. The Source Distribution Coefficient for Various Nozzle Pressure Ratios as a Function of Nozzle Radius. Sonic Nozzle, $\gamma = 1.4$

The integration is most conveniently carried out if we use the dummy variable

$$z = x - x_j \qquad \text{so} \quad x_j = x - z$$

(Note that z differs by βr from the value used in Appendix A.)

$$\text{Then } r = r_j + \delta_j (x - z) - \frac{\delta_j (x^2 - 2xz + z^2)}{2x_{jm}}$$

$$= \left[r_j + \delta_j x \left(1 - \frac{x}{2x_{jm}} \right) \right] - \delta_j \left(1 - \frac{x}{x_{jm}} \right) z - \frac{\delta_j}{2x_{jm}} z^2$$

$$= A - Bz - Cz^2 \qquad \text{say} \tag{31}$$

$$\therefore q(z) = 2\pi u_o r \frac{dr}{dz} = -2\pi u_o (A - Bz - Cz^2)(B + 2Cz)$$

$$= -2\pi u_o (a + bz + ez^2 + fz^3) \qquad \text{say} \tag{32}$$

$$\text{when } a = AB = \delta_j x_{jm} \left[\breve{r}_j + \delta_j \breve{x} \left(1 - \tfrac{1}{2} \breve{x} \right) \right] (1 - \breve{x})$$

$$b = -(B^2 - 2AC) = -\delta_j{}^2 (1 - \breve{x})^2 + \delta_j \left[\breve{r}_j + \delta_j \breve{x} \left(1 - \tfrac{1}{2} \breve{x} \right) \right]$$

$$e = -3BC = -\frac{3}{2} \frac{\delta_j{}^2}{x_{jm}} (1 - \breve{x})$$

$$f = -2C^2 = -\frac{1}{2} \frac{\delta_j{}^2}{x_{jm}{}^2}$$

where

$$\breve{x} = x/x_{jm} \qquad \breve{r}_j = r_j/x_{jm}$$

We can now determine the velocity pertubations from Appendix A From equation A4, noting that $dz = -dx_j$ the axial pertubation is

$$\frac{u}{u_o} = \frac{1}{2}\int_{z_o}^{z_1} \frac{\left(az + bz^2 + ez^2 + fz^4\right) dz}{\left(z^2 + \beta^2 r^2\right)}$$

$$= \frac{1}{2}\left[-\frac{1}{\sqrt{z^2 + \beta^2 r^2}}\left(a + bz - e\beta^2 r^2 - fz\beta^2 r^2\right)\right.$$

$$+ \sqrt{z^2 + \beta^2 r^2}\left(e + \frac{1}{2}fz\right)$$

$$\left. + \left(b - \frac{3}{2} f\beta^2 r^2\right) \log\left(z + \sqrt{z^2 + \beta^2 r^2}\right)\right]_{z_o}^{z_1} \qquad (33)$$

From equation A5, the radial velocity pertubation is given by

$$\frac{v}{u_o} = \frac{\beta^2 r}{2}\int_{z_o}^{z_1} \frac{\left(a + bz + ez^2 + fz^3\right) dz}{\left(z^2 + \beta^2 r^2\right)^{3/2}}$$

$$= \frac{\beta^2 r}{2}\left[\frac{1}{\sqrt{z^2 + \beta^2 r^2}}\left(\frac{az}{\beta^2 r^2} - b - ez + f\beta^2 r^2\right)\right.$$

$$\left. + f\sqrt{z^2 + \beta^2 r^2} + e \log\left(z + \sqrt{z^2 + \beta^2 r^2}\right)\right]_{z_o}^{z_1} \qquad (34)$$

While one could formally proceed to expand these equations, the form given is most suitable for numerical evaluation. The limits are $z_1 = x - x_{jm}$ and $z_o = x$. While this "exact" solution may be of research

interest, its usefulness is limited by the slender body approximations employed to define $q(x_j)$. It cannot be accurate, or even close, when δ_j is large. We may as well employ equation (30) therefore, so that

$$q(z) = 2\pi u_o r_j \delta_j \left(1 - \frac{x - z}{x_{jm}}\right) \tag{35}$$

$$\therefore \quad a = - r_j \delta_j (1 - \breve{x}) \qquad (\breve{x} = x/x_{jm}, \text{ etc.})$$

$$b = - \frac{r_j \delta_j}{x_{jm}}$$

Than from equation (33), inserting the limits

$$\frac{\Delta u}{u_o} = \frac{- \frac{1}{2} \breve{r}_j \delta_j}{\sqrt{\breve{x}^2 + \beta^2 \breve{r}^2}} \left\{ 1 + \sqrt{\breve{x}^2 + \beta^2 \breve{r}^2} \log \left[\frac{\breve{x} - 1 + \sqrt{(\breve{x} - 1)^2 + \beta^2 \breve{r}^2}}{\breve{x} + \sqrt{\breve{x}^2 + \beta^2 \breve{r}^2}} \right] \right\} \tag{36}$$

$$\text{and } C_p \approx - 2 \frac{\Delta u}{u_o}$$

Again, because of limited accuracy, we may as well neglect $(v/u_o)^2$ in relation to $\Delta u/u_o$. Then we find that the change in C_p due to the plume is

$$\frac{\Delta C_p}{\hat{r}_j \delta_j} = f\left[x_1 \quad (\beta r)^2\right] \tag{37}$$

Often, a more useful form is in terms of $\hat{x} = x/r_j$, $\hat{r} = r/r_j$. Then

$$\frac{\Delta u}{u_o} = \frac{- \frac{1}{2} \delta_j}{\sqrt{\hat{x}^2 + \beta^2 \hat{r}^2}} \left\{ 1 + \frac{\delta_j}{2} \frac{\sqrt{\hat{x}^2 + \beta^2 \hat{r}^2}}{\left(\hat{r}_m - 1\right)} \log \left[\frac{\hat{x} - 1 + \sqrt{(\hat{x} - 1)^2 + \beta^2 \hat{r}^2}}{\hat{x} + \sqrt{\hat{x}^2 + \beta^2 \hat{r}^2}} \right] \right\} \tag{38}$$

But this introduces the additional terms in δ_j and r_m/r_j, which depend upon p_{jt}/p_∞, so for a simple overview of the plume effect, equation (36), as presented in contour in Figure 24, is often preferable.

It is clear from both forms of the equation that a simple integral (like Φ in the section on entrainment) cannot be derived to account for the plume effect. The change in boattail drag, due to the plume, will be

$$\Delta C_{Dp} = \frac{1}{\pi} \int_{r_j}^{r_m} \Delta C_{p_p} \; 2\,\hat{r}\,d\hat{r}$$

$$\text{where } \Delta C_{p_p} = \frac{\delta_j}{\sqrt{\hat{x}^2 + \beta^2\hat{r}^2}} \left\{ 1 + \frac{\delta_j}{2} \frac{\sqrt{\hat{x} + \beta^2\hat{r}^2}}{\left(\hat{r}_m - 1\right)} \log\left[\frac{\hat{x} - 1 + \sqrt{(\hat{x} - 1)^2 + \beta^2\hat{r}^2}}{\hat{x} + \sqrt{\hat{x}^2 + \beta^2\hat{r}^2}} \right] \right\} \qquad (39)$$

and both δ_j and $\hat{r}_m$ are functions of p_{jt}/p_∞, as given earlier.

So even this very approximate formulation must be numerically integrated. That being so, one might as well employ the complete slender body equations to compute ΔC_{p_p}. This has been done in a Fortran conversational program PLUME3 listed in Appendix B. The program also includes the entrainment effects discussed earlier, equation (17). A comparison of the program output with experiment is given in Figures 25 and 26.

As might be expected, there is some disagreement in the absolute values of C_p, particularly close to the jet, because our inviscid flow theory neglects the boundary layer displacement thickness. But the change in C_p due to the plume effect appears to be correct.

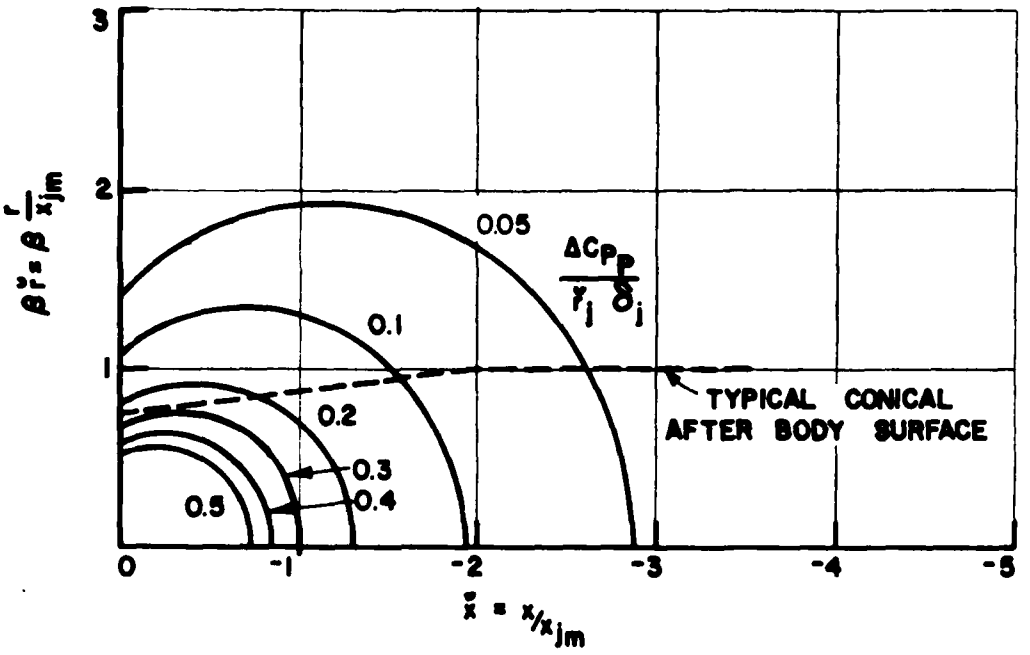

Figure 24. Contours of $\frac{\Delta C_{p_p}}{\breve{r}_j \delta_j}$ in $\breve{x}$ and $\breve{r}$. ΔC_{p_p} is the change in boattail pressure due to the plume shape.

x_{jm} = downstream distance from the jet exit to the maximum plume diameter.

$-x$ = upstream distance from the jet exit plane.

r = local boattail radius.

β = $\sqrt{1 - M^2}$

δ_j = jet turning angle at the nozzle.

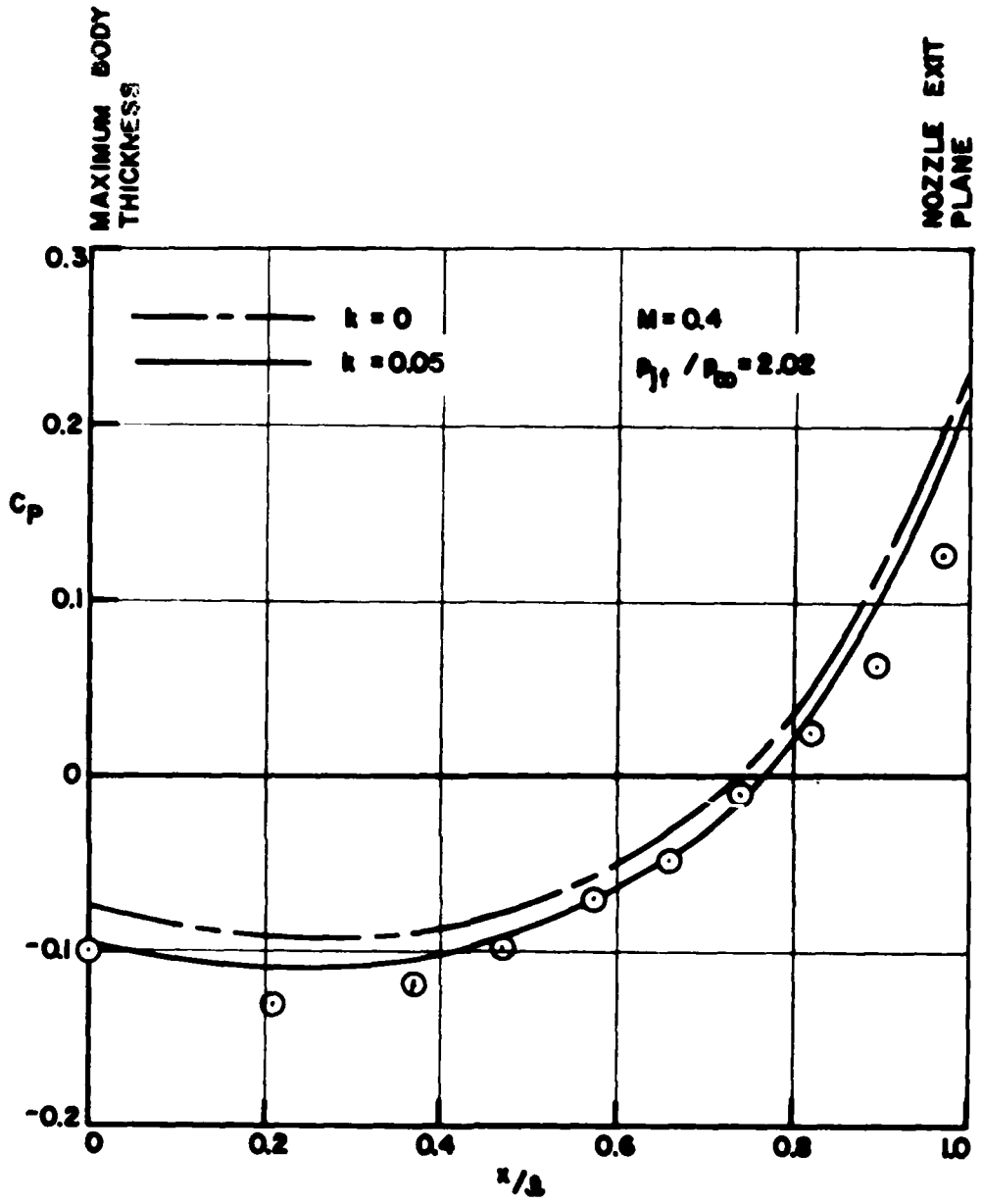

Figure 25. A Comparison Between Theory and Experiment for M = 0.4 Data of Reubush and Runkel.[11] Configuration 3 afterbody. (Theory from PLUME 3 program.)

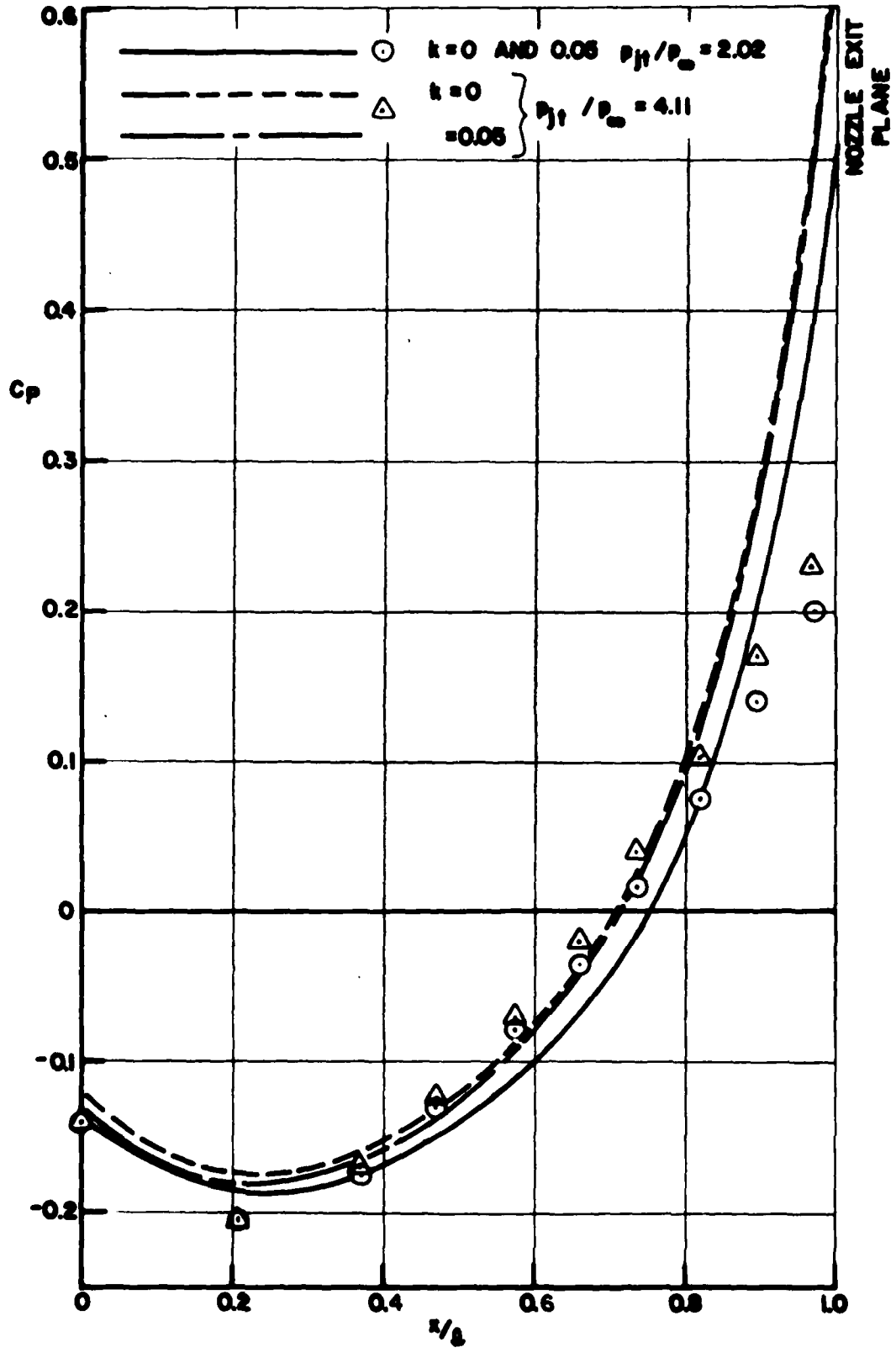

Figure 26. A Comparison Between Theory and Experiment for M = 0.9. Data of Reubush and Runkel.[11] Configuration 3 afterbody. (Theory from PLUMES 3 Program.)

SUMMARY AND CONCLUSIONS

A theoretical framework has been presented for the prediction of the change in boattail drag with nozzle pressure ratio (NPR) and agreement with experiment seems good in those few cases where it was possible to check. The most severe restrictions are

- No base area
- Attached flow with negligible boundary layer (BL) thickness.

The second of these would be fairly simple to relax, by incorporating axisymmetric BL equations. We would then have a tool which permitted the optimum shape for particular internal volume constraints to be determined on the computer. Perhaps more importantly, it would enable unsatisfactory shapes to be identified and modified before testing.

REFERENCES

1. Grossman, B. and R.E. Melnik, "The Numerical Computation of the Transonic Flow Over Afterbodies Including the Effect of Jet-Plume and Viscous Interactions." AIAA Paper 75-62, January 1975.

2. Riegels, F. and H. Eggert, "Messungen am Heck von Strahlgondein." Deut. Luftfahrtforschung U.M. 3201, 1944.

3. Kuchemann, D. and J. Weber, Aerodynamics of Propulsion. New York: McGraw-Hill Book Company, Inc., 1953.

4. Moulden, T.H., J.M. Wu, and D.J. Spring, "Model of the Engine Exhaust System at Transonic Flight Speeds." Journal of Spacecraft, Vol. 12, No. 7, July 1975.

5. Chow, W.L., L.J. Bober and B.H. Anderson, "Strong Interaction Associated with Transonic Flow Past Boattailed Afterbodies." AIAA Journal Vol. 13, No. 1, January 1975.

6. Smoot, L.D., "Turbulent Mixing Coefficients for Compressible Coaxial Submerged and Coflowing Jets." AIAA Journal, Vol. 14, No. 12, December 1976.

7. Albertson, M.L., Y.B. Dai, R.A. Jensen and H. Rouse, "Diffusion of Submerged Jets." Paper No. 2409, American Society of Civil Engineers, Transactions, Vol. 115, 1950.

8. Reubush, D.E., "Effects of Fineness and Closure Ratios on the Boattail Drag of Circular-Arc Afterbody Models with Jet Exhaust at Mach Numbers Up to 1.3." NASA TND-7163, May 1973.

9. Love, E.S., C.E. Grigsby, L.P. Lee and M.J. Woodling, "Experimental and Theoretical Studies of Axisymmetric Free Jets." NASA TRR-6, 1959.

10. Vick, A.R., E.H. Andrews, Jr., J.S. Dennard and C.B. Craidon, "Comparisons of Experimental Free-Jet Boundaries with Theoretical Results Obtained with the Method of Characteristics." NASA TND-2327, June 1964.

11. Reubush,D.E. and J.F. Runckel, "Effect of Fineness Ratio on the Boattail Drag of Circular-Arc Afterbodies Having Closure Ratios of 0.50 with Jet Exhaust at Mach Numbers Up to 1.30." NASA TN D-7192, May 1973.

APPENDIX A

DERIVATION OF THE SUBSONIC SLENDER BODY EQUATIONS FOR A BODY AT ZERO INCIDENCE

(In this appendix, the perturbation velocities Δu, Δv are written as u, v for conciseness. Also, ψ is the familiar stream function
ϕ is the velocity potential)

The Representation of a Body by Singularities

As was first suggested by Rankine[A1] the axi-symmetric flow about large classes of bodies can be represented by distributions of sources and sinks (negative sources) along their axes. If the total strength (Q) of the sources and sinks is zero, the streamline representing the body will be closed; if not, it will be semi-infinite, the extension to infinity being downstream if the total strength Q>0, and upstream if Q<0.

The velocity potential ϕ and stream function ψ for a single source of strength Q (ft^3/sec) at the origin in terms of cylindrical coordinates (r,x) is

$$\phi = \frac{-Q}{4\pi\sqrt{r^2 + x^2}}$$

and the stream function is

$$\psi = \frac{-Qx}{4\pi\sqrt{r^2 + x^2}}$$

One can also (or alternatively) employ higher order singularities, when convenient. By differentiating the above equation with respect to x we obtain the values of ϕ and ψ for a source doublet: viz

$$\phi = \frac{-Qx}{4\pi\left(r^2 + x^2\right)^{3/2}}$$

$$\psi = \frac{-Qr^2}{4\pi\left(r^2 + x^2\right)^{3/2}}$$

Further differentiation will yield singularities of higher order at the origin.

More general classes of body shape may be calculated using source or vortex rings or discs, discrete or continuous, either "buried" below or at the stream surface which represents the body. In general, these more sophisticated singularities involve somewhat more complex analysis (particularly when the flow is compressible) and these complications are not necessary for the present problem.

The General Distributed Source Body in Subsonic Flow

Small pertubation theory in subsonic three-dimensional flow gives the velocity potential of a point source located on the x axis as [A2]

$$\phi = -\frac{m}{4\pi}\frac{1}{\sqrt{(x - x_1)^2 + \beta^2 r^2}} \tag{A1}$$

where $r^2 = y^2 + z^2$

$\beta^2 = 1 - M^2$

m = the source strength (negative for a sink)

M = the free stream Mach number

x_1 = location of the source on the x axis

The velocity perturbations u and v (in the x - direction and radially normal to it) associated with the source are therefore

$$u = \frac{\partial\phi}{\partial x} = \left(\frac{m}{4\pi}\right)\frac{(x - x_1)}{\left[(x - x_1)^2 + \beta^2 r^2\right]^{3/2}} \tag{A2}$$

$$v = \frac{\partial\phi}{\partial r} = \left(\frac{m}{4\pi}\right)\frac{\beta^2 r}{\left[(x - x_1)^2 + \beta^2 r^2\right]^{3/2}} \tag{A3}$$

For a continuous distribution of sources $q(x_1)$ between $x = a$ and $x_1 = b$, it follows that

$$m = q(x_1)dx_1$$

$$u = \frac{1}{4\pi}\int_a^b q(x_1)\frac{(x - x_1)}{\left[(x - x_1)^2 + \beta^2 r^2\right]^{3/2}}dx_1 \tag{A4}$$

$$v = \frac{1}{4\pi}\int_a^b q(x_1)\frac{\beta^2 r}{\left[(x - x_1)^2 + \beta^2 r^2\right]^{3/2}}dx_1 \tag{A5}$$

Let $z = \dfrac{x - x_1}{\beta r}$ (so that $\dfrac{dz}{dx_1} = \dfrac{-1}{\beta r}$)

$$\text{Then } u = \frac{-1}{4\pi\beta r} \int_{z_a}^{z_b} q(z) \frac{z}{\left(1 + z^2\right)^{3/2}} dz \tag{A6}$$

$$v = \frac{-1}{4\pi r} \int_{z_a}^{z_b} q(z) \frac{dz}{\left(1 + z^2\right)^{3/2}} \tag{A7}$$

Integration by parts enables us to express the velocity components as a series in $\dfrac{d^n q(z)}{dz^n}$ plus a residual integral. The first few terms are

$$u = -\frac{1}{4\pi\beta r} \left\{ -\frac{q}{\sqrt{1 + z^2}} + \frac{dq}{dz} \log\left(z + \sqrt{1 + z^2}\right) - \frac{d^2q}{dz^2} \left[z \log\left(z + \sqrt{1 + z^2}\right) - \sqrt{1 + z^2} \right] \right\}_{z_a}^{z_b}$$

$$+ \frac{1}{4\pi\beta r} \int_{z_a}^{z_b} \frac{d^3q}{dz^3} \left[z \log\left(z + \sqrt{1 + z^2}\right) - \sqrt{1 + z^2} \right] dz \tag{A8}$$

$$v = -\frac{1}{4\pi r} \left\{ \frac{qz}{\sqrt{1 + z^2}} - \frac{dq}{dz}\sqrt{1 + z^2} + \frac{1}{2} \frac{d^2q}{dz^2} \left[z\sqrt{1 + z^2} + \log\left(z + \sqrt{1 + z^2} \right) \right] \right\}_{z_a}^{z_b}$$

$$- \frac{1}{2r} \int_{z_a}^{z_b} \frac{d^3q}{dz^3} \left[z\sqrt{1 + z^2} + \log\left(z + \sqrt{1 + z^2} \right) \right] dz \tag{A9}$$

In other words, the flow field is defined by the nature of the source line at each end.* If the third derivative of the source strength is zero at its ends, equations (A8) and (A9) give the flow field explicitly; and, of course, the equations can be extended to higher order derivatives by further integration by parts.

In passing, it's of interest to note that the simplest possible body of this type (apart from the limit case of a sphere) is given by

$$q = q_o - q_1 x_1 \tag{A10}$$

for the body to be closed

$$Q = \int_o^{x_b} q\,dx_1 = q_o x_b - \tfrac{1}{2} q_1 x_b^2 = 0$$

$$\therefore \quad x_b = \frac{2q_o}{q_1} \qquad q_o - q_1 x_b = -q_o$$

From equations (A8) and (A9):

$$u = \frac{q_o}{4\pi}\left\{\frac{1}{\sqrt{x^2 + \beta^2 r^2}} - \frac{1}{\sqrt{(x - x_b)^2 + \beta^2 r^2}} - \frac{2}{x_b} \log\left[\frac{x + \sqrt{x^2 + \beta^2 r^2}}{(x - x_b) + \sqrt{(x - x_b)^2 + \beta^2 r^2}}\right]\right\} \tag{A11}$$

$$v = \frac{q_o}{4\pi r}\left[-\frac{\beta x}{\sqrt{x^2 + \beta^2 r^2}} + \frac{(x - x_b)}{\sqrt{(x - x_b^2)^2 + \beta^2 r^2}} + \frac{2}{x_b}\sqrt{x^2 + \beta^2 r^2} - \frac{2}{x_b}\sqrt{(x - x_b)^2 + \beta^2 r^2}\right] \tag{A12}$$

*This is the reason why not all body shapes can be represented by this type of singularity.

At the midpoint, $x = \frac{1}{2}x_b$, $v = o$ and

$$u = \frac{q_o}{2\pi x_b} \log \left[\frac{\sqrt{1 + (2\beta r/x_b)^2} + 1}{\sqrt{1 + (2\beta r/x_b)^2} - 1} \right] \tag{A13}$$

For any body, the boundary condition at the surface is

$$\frac{v}{u_o + u} = \frac{dr}{dx} = \frac{dr}{dz}\frac{dz}{dx_1} = -\frac{1}{\beta r}\frac{dr}{dz} \tag{A14}$$

So since $\frac{dr}{dz}$ is known, we can in principle solve for q(z), the source distribution required to give r(z). In practice it is easier to seek the desired shape iteratively.

The resultant velocity is

$$V = \sqrt{(u_o + u)^2 + v^2} \tag{A15}$$

Thus, from Bernoulli, the local static pressure p is given by

$$p_\infty + \frac{1}{2}\rho_\infty u_o^2 = p + \frac{1}{2}\rho_\infty \left[(u_o + u)^2 + v^2 \right]$$

$$\therefore C_p = \frac{p - p_\infty}{\frac{1}{2}\rho_\infty u_o^2} = -\left[2\frac{u}{u_o} + \left(\frac{u}{u_o}\right)^2 + \left(\frac{v}{u_o}\right)^2 \right] \tag{A16}$$

Note that the $\left(\frac{u}{u_o}\right)^2$ term can generally be disregarded in evaluating (A16), but not always $\left(\frac{v}{u_o}\right)^2$. This is because $\left(\frac{v}{u_o}\right)$ is often much larger than $\left(\frac{u}{u_o}\right)$.

The Slender Body Approximation

"Slender body" theory assumes that the body is so slender that $\beta r << (x - x_1)$ and $u << u_o$. Thus, from equation (A14)

$$\frac{dr}{dx} \simeq \frac{v}{u_o} \tag{A17}$$

Following the early work of investigators such as Laitone[A4], Ward[A2], Neumark[A6] and Adams and Sears[A7]

$$q(x_1) \propto u_o \frac{dS}{dx_1} = 2\pi u_o r \frac{dr}{dx_1} \qquad \text{(A18)}$$

where S is the local body cross-sectional area πr^2, and assuming that there are no local discontinuities in dr/dx_1, then

$$q(z) = -\frac{2\pi u_o}{\beta}\left(\frac{dr}{dz}\right) \qquad \left(\text{as } \frac{dz}{dx_1} = -\frac{1}{\beta r}\right) \qquad \text{(A19)}$$

Using (A18) in conjuction with (A4) and (A5) or (A19) with (A6) and (A7) solutions for u and v are readily obtained. Analytic solutions are possible for simple body shapes, but numerical integration of (A4) and (A5) is extremely simple, and is much to be preferred for general purposes.

The Tapered Sting Problem

This was first essayed by Tunnell[A3] using the slender body equations of Laitone.[A4] These equations neglect the radial velocity pertubation (v), which we will include.

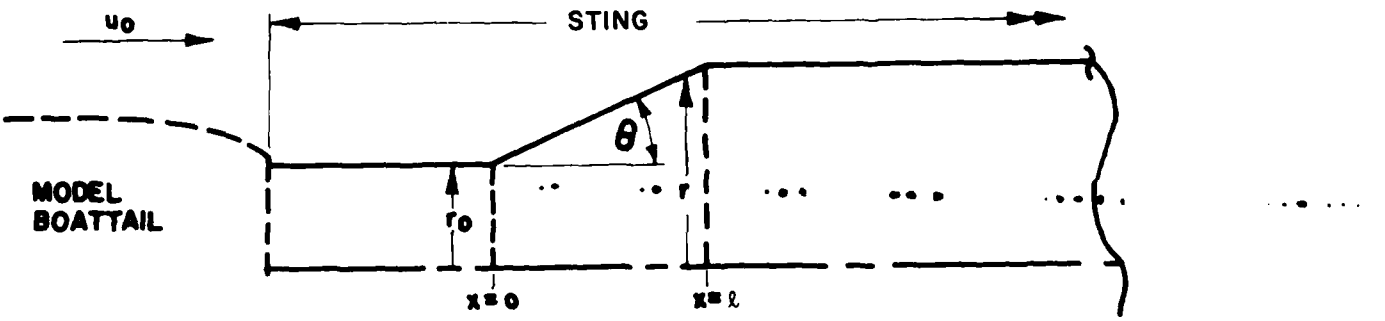

For $o < x < \ell$, $r = r_o + x \tan \theta$. To calculate the effect of the sting taper on the model pressure distribution, we need to solve for C_p in the region $x < o$.

This is directly related to a more general problem; that of computing the inviscid pressure distribution over the surface of a conical afterbody, and the change in pressure it induces elsewhere. In the notation of the sketch above, the solution is

$$\frac{u}{u_o} = -\frac{1}{2}\tan\theta\left\{\frac{r_o}{\sqrt{x^2+\beta^2r^2}} - \frac{(r_o+\ell\tan\theta)}{\sqrt{(x-\ell)^2+\beta^2r^2}} - \tan\theta\,\log\left[\frac{x-\ell+\sqrt{(x-\ell)^2+\beta^2r^2}}{x+\sqrt{x^2+\beta^2r^2}}\right]\right\} \tag{A20}$$

$$\frac{v}{u_o} = -\frac{1}{2}\tan\theta\left\{\frac{x-\ell+\beta^2r\tan\theta}{\sqrt{(x-\ell)^2+\beta^2r^2}} - \frac{x+\beta^2r^2\tan\theta}{\sqrt{x^2+\beta^2r^2}}\right\} \tag{A21}$$

$$C_p = -[2(u/u_o) + (u/u_o)^2 + (v/u_o)^2] \tag{A16}$$

(When using these equations for a conical boattail, it should be remembered that θ will be <u>negative</u>, in contrast to the usual convention.) If we write $r = r_o$, equation A20 is identical with Tunnell's, as would be expected.

Tunnell obtained a solution for $r = r_o$, since he was only interested in the effect of the sting taper on base pressure. Figure A1 gives a comparison of his equation with those above, and his experimental data. Both analyses neglect the boundary layer displacement thickness over the model and the sting. In particular, the boundary layer will reduce the effective angle θ of the sting taper, and increase r_o; both of which would reduce the theoretical values of ΔC_{p_b} slightly, especially in the vicinity of the discontinuity.

Since the sting taper was always present in Tunnell's experiments, we have no means of knowing the "baseline" value to subtract in order to get ΔC_p, the change due to the taper. But the theory should be most accurate when the taper is furthest removed from the base; so this value of ΔC_p is used to compute the baseline value.

Note that by integrating equation A16 over a boattail, we can determine the effect of a tapered sting on C_{p_β} as well as C_{p_b}.

Figure A2 compares equations A20-A21 with measured pressure distributions over a conical boattail. Agreement is rather poor in this case. Near $x = 0$ the discontinuity in r causes a large suction "spike" which slender body theory cannot predict. (Shape discontinuities cannot be produced by any combination of singularities on the axis of symmetry.) And the combined

effects of jet entrainment and boundary layer growth (mostly the latter) prevent the full recompression being achieved near the exhaust plane.

Comparison Between Slender Body Theory and Exact Solutions

Several authors have compared slender body theory with Lamb's[A5] exact solution for a spheroid. The horizontal velocity disturbance at the point of maximum thickness, for example, is given by Lamb as

$$\left.\frac{u}{u_o}\right|_{max} = \frac{\delta^2(\log e + 2f)}{2f - \delta^2 \log e}$$

where

$$f = \sqrt{1 - (r_m/a)^2} \qquad (a = \text{semi-major axis})$$

$$e = \frac{1 + f}{1 - f}$$

Slender body theory, on the other hand, gives

$$\left.\frac{u}{u_o}\right|_{max} = \frac{1}{2}(r_m/a)^2 \log\left[\frac{1 + \sqrt{1 + (r_m/a)^2}}{-1 + \sqrt{1 + (r_m/a)^2}}\right]$$

The corresponding values of u/u_o are tabulated below.

r_m/a	Exact solution	Slender Body Theory
.0001	8.9×10^{-8}	9.9×10^{-8}
.001	6.6×10^{-6}	7.6×10^{-6}
.01	4.3×10^{-4}	5.3×10^{-4}
.1	.0207	.03
.2	.0591	.0925

The discrepancy here is due to the fact that, no matter how low its thickness to chord ratio, the ends of a spheroid are not "slender" and introduce large errors into the equation. So the comparison is not really valid. A more appropriate comparison would require the exact solution to be for a body with pointed ends, or for a nondiscountinuous change in the diameter of an infinite body.

APPENDIX A REFERENCES

A1. Rankine, W.J.M. — "On the Mathematical Theory of Streamlines, Especially Those With Four Foci Upwards." Phil. Trans. 161, P-267 (1871).

A2. Ward, G.N. — "Linearized Theory of Steady High-Speed Flow." Cambridge University Press, P-39 (1955).

A3. Tunnell, P.J. — "An Investigation of Sting-Support Interference on Base Pressure and Forebody Chord Force at Mach Numbers from 0.6 to 1.30." NACA RM A54K16a (January 1955).

A4. Laitone, E.V. — "The Subsonic Flow About a Body of Revolution." Quart. Appl. Math., Vol. V., No. 2 (July 1947).

A5. Lamb, Sir Horace — Hydrodynamics, Sixth Edition. New York: Dover Publications (1945).

A6. Neumark, S. — "Velocity Distribtuion on Thin Bodies of Revolution at Zero Incidence in Incompressible Flow." Rep. Memor. Aero Res. Coun., 2814, (1950).

A7. Adams, MacC., and Sears, W.R. — "Slender Body Theory - Review and Extension." J. Aero Sci., 20, 85, (1953).

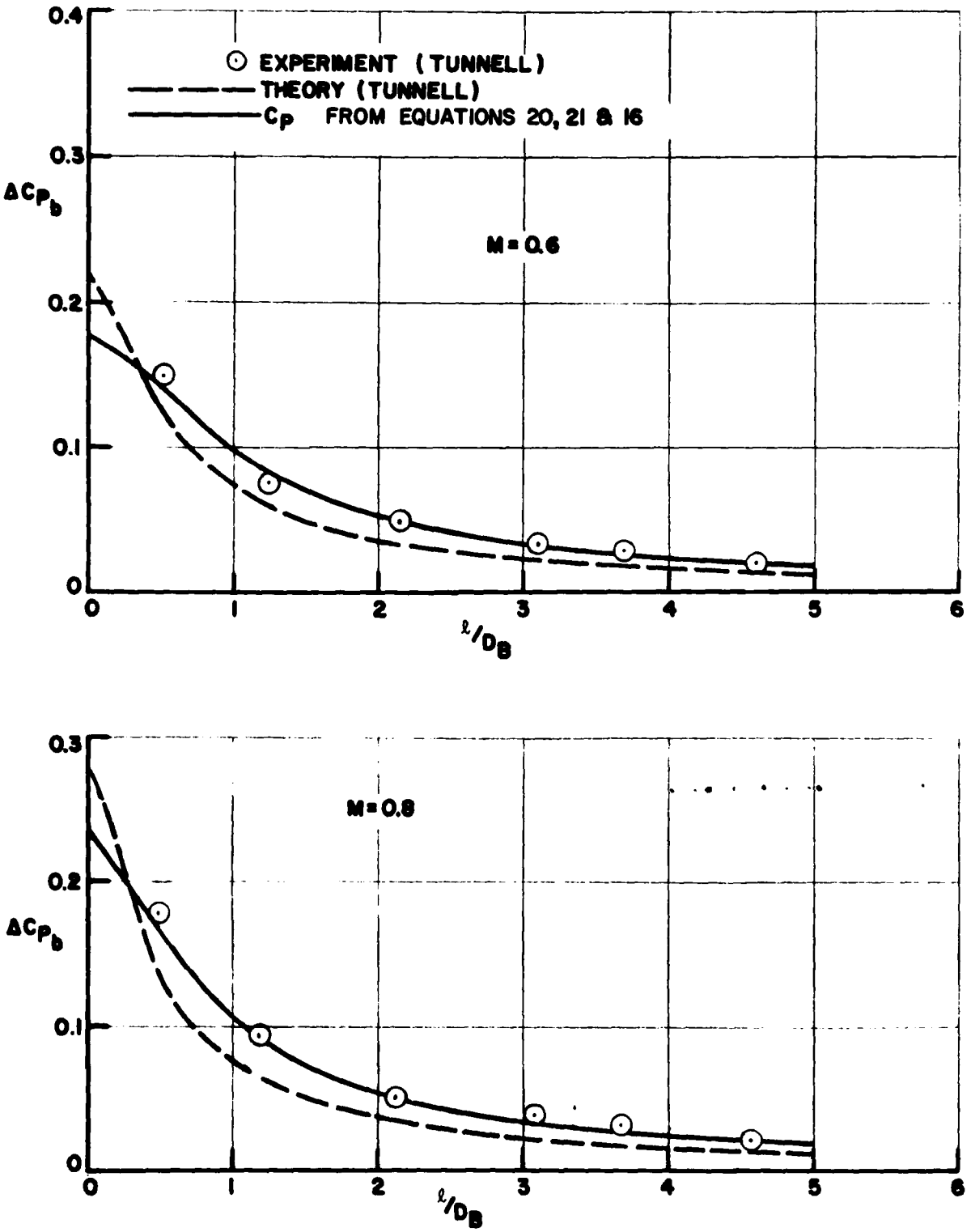

Figure A1. The Change in Base Pressure Due to a Tapered Sting; a Comparison between Tunnell's Experiments and Slender Body Theory.

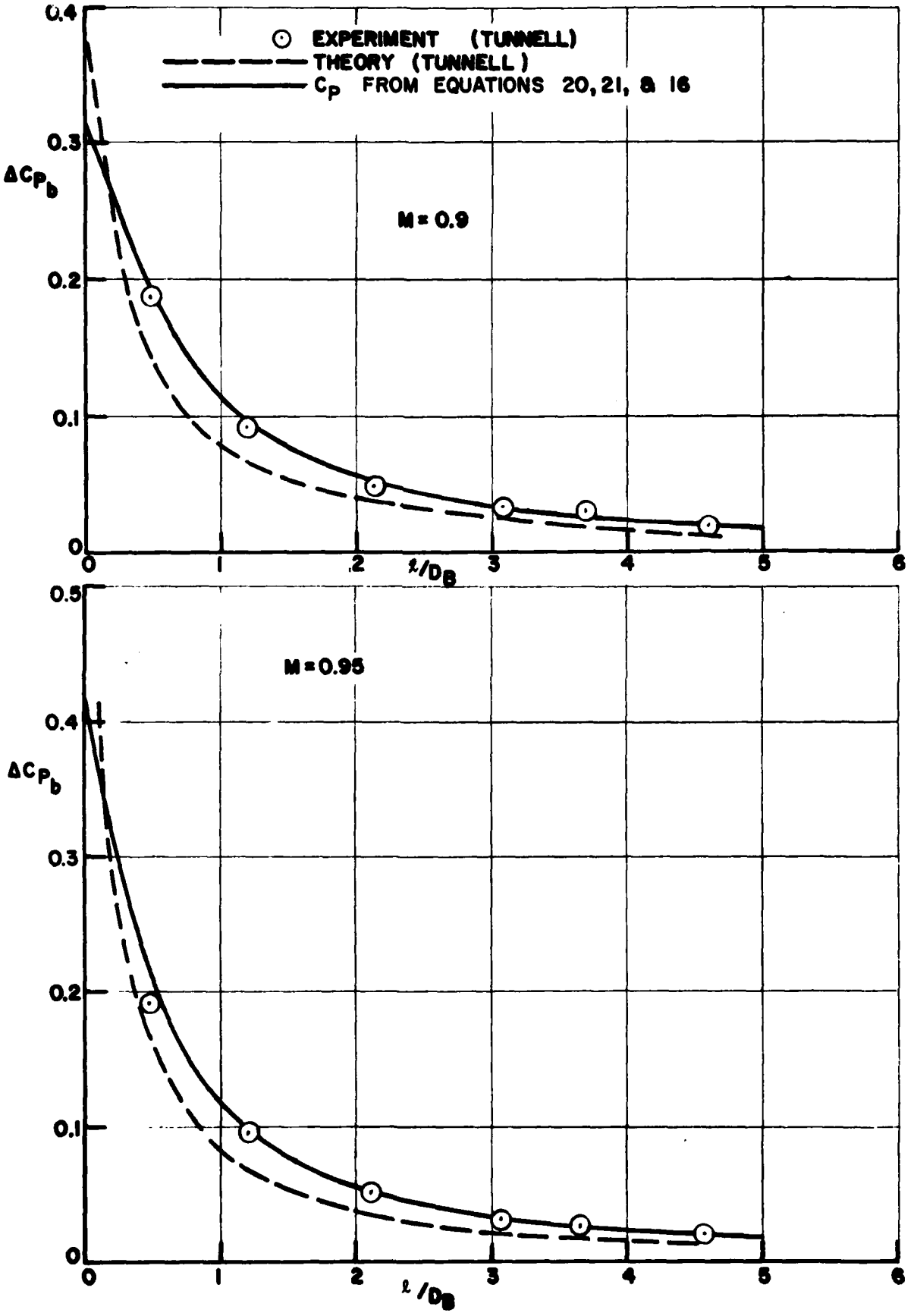

Figure A1. (continued)

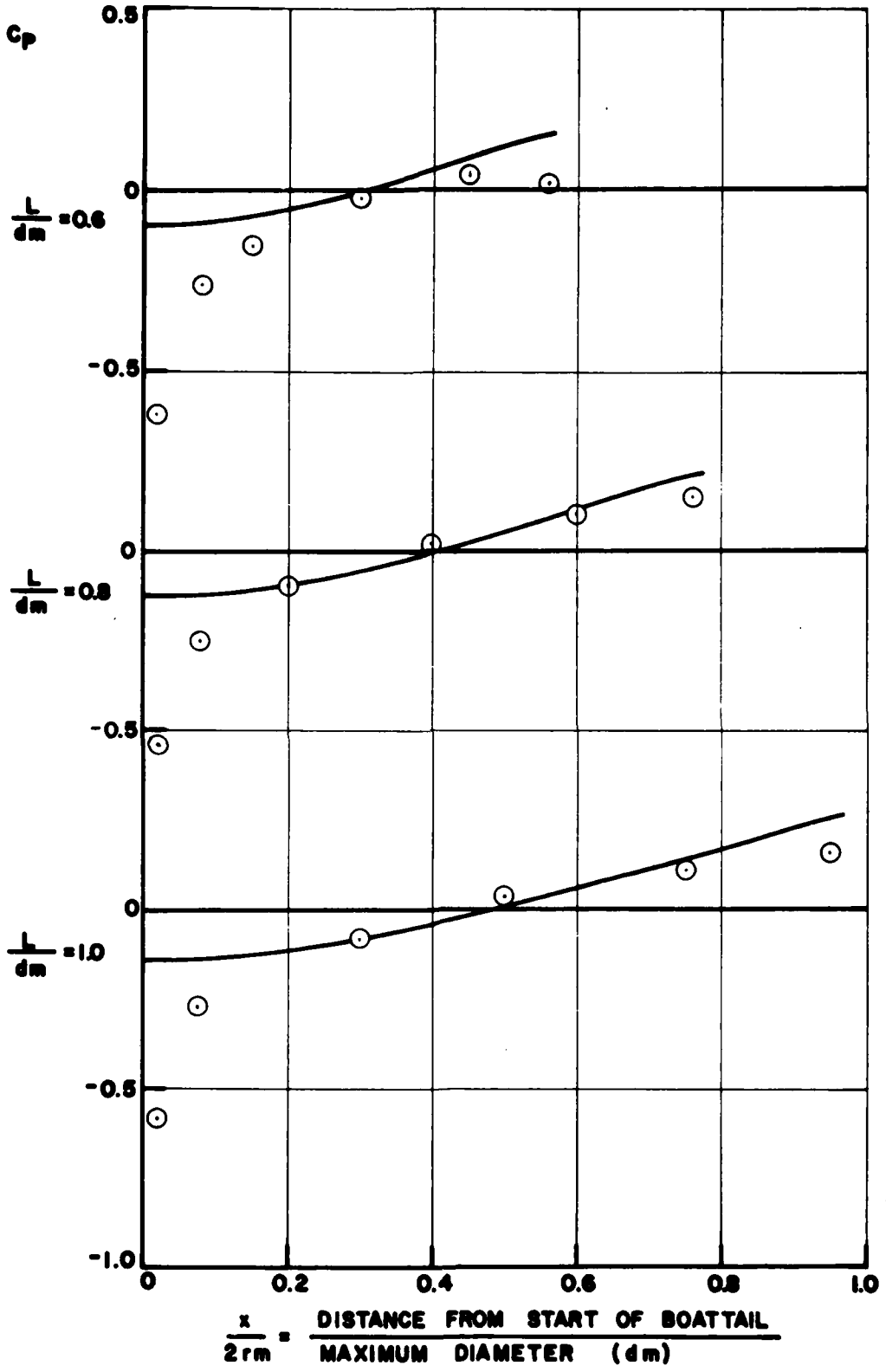

Figure A.2. Conical afterbody pressure distribution at M = 0.4. A comparison with slender body theory (no plume or entrainment) with experimental data for p_{jt}/p_{∞} = 2.0. (Data from Compton and Runckel)

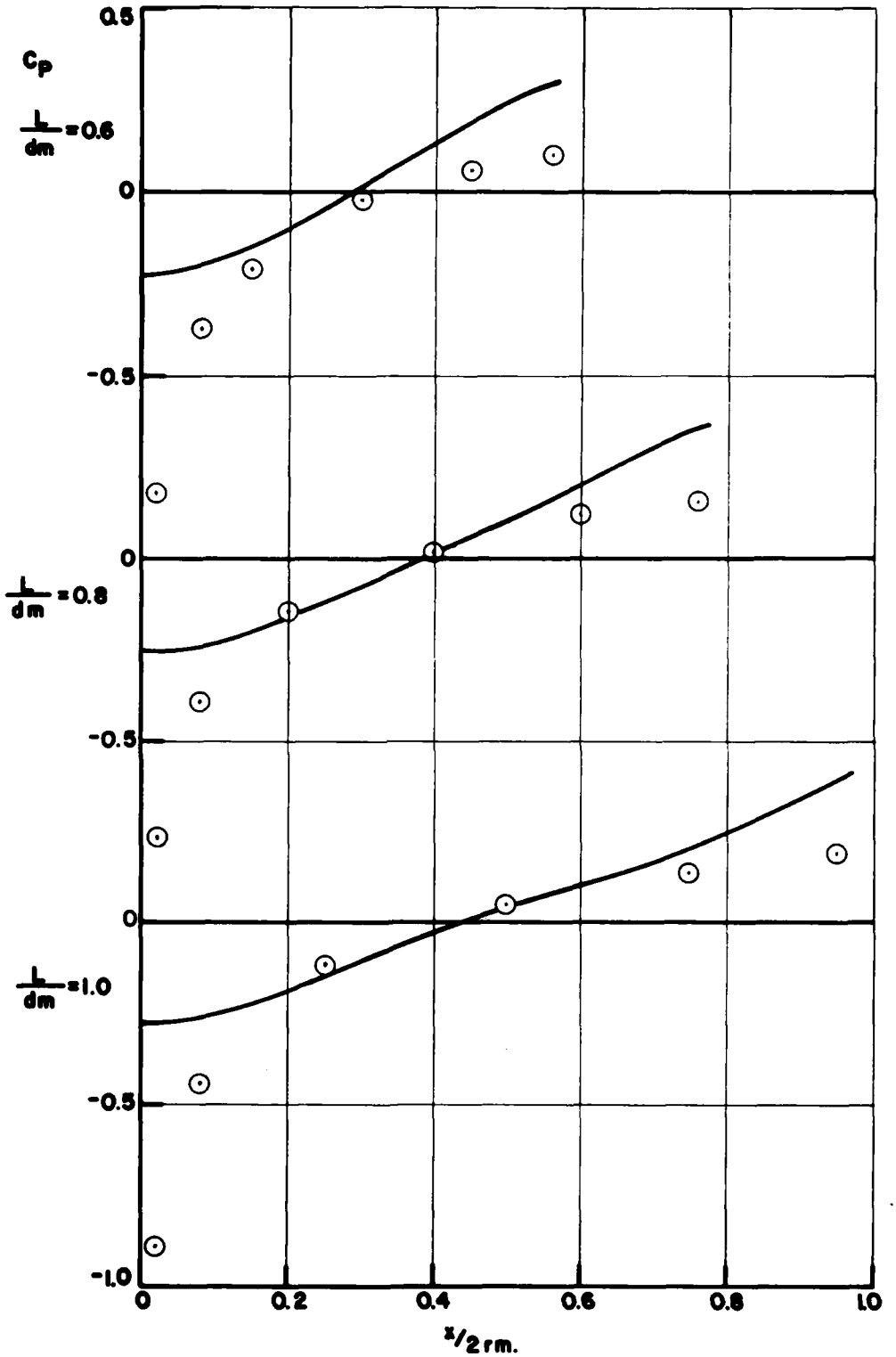

Figure A.2. (Continued) M = 0.8.

APPENDIX B. PROGRAM "PLUME3"

This program uses equations (17), (33) and (34) to compute the pressure distribution over circular arc boattails. The arc size can be anywhere between infinity (which gives a conical boattail, of course) and the minimum which fits tangentially to the forebody and gives the correct surface angle θ at the nozzle exit plane. In retrospect, it would have been better to have used a power series representation, since slender body theory breaks down when the surface is discontinuous. Thus only the tangential arc case is really usable in this program. However, the modifications required to generalize the boattail shape are relatively straight-forward.

The program is "conversational," a typical output being shown in Table B.1. The only difference between these two runs is that k = 0 in the first and k = .05 in the second. The inputs are

R-M = r_m, the maximum body radius
R-J = r_j, the initial jet radius
L-BETA = the length of the afterbody
P = NPR, the nozzle pressure ratio
GAMMA = γ, the ratio of specific heats in the jet
K = k, the entrainment coefficient
VS = a, the speed of sound in the jet
M = M, the free stream Mach number.

Table B.2 lists the program.

Table B.1.

```
DO YOU WANT A NEW RUN?  TYPE YES OR NO.
!YES
NEW VARIABLE?  !M,.9
NEW VARIABLE?  !NO,1
INPUT VARIABLES FOR THIS RUN

    R-M          R-J          L-BETA       P            GAMMA
     1            .5           3.536        2.02         1.4

    K            VS           M            N            N1
     0          1117             .9       40           200

    KSI
     1

CALCULATED PARAMETERS FOR THIS RUN

     R-P         THETA-J      BODY RADIUS PLUME RADIUS  PLUME TERM
      .501212  .970882E-02     12.7532   10618.5         106.627


     X            U/U-0         V/U-0         C-P           C-D INT

     0          .620742E-01 -.142390E-01      -.128204 -.313574E-07
      .3536     .800171E-01 -.321110E-01      -.167468  .194095E-02
      .7072     .870689E-01 -.554903E-01      -.184798  .762218E-02
     1.0608     .850697E-01 -.807544E-01      -.183897  .168544E-01
     1.4144     .759378E-01     -.10685       -.169059  .285567E-01
     1.768      .601045E-01     -.133474      -.141637  .410201E-01
     2.1216     .368033E-01     -.160467      -.100711  .520145E-01
     2.4752     .353787E-02     -.187509 -.422479E-01   .587809E-01
     2.8288    -.467444E-01     -.213283  .458143E-01   .577164E-01
     3.1824       -.13956       -.229367      .207034   .427128E-01
     3.536        -.314962      -.144381      .509877   .131749E-02
```

```
DO YOU WANT A NEW RUN?  TYPE YES OR NO.
!YES
NEW VARIABLE?  !K,.05
NEW VARIABLE?  !NO,1
INPUT VARIABLES FOR THIS RUN

    R-M          R-J          L-BETA       P            GAMMA
     1            .5           3.536        2.02         1.4

    K            VS           M            N            N1
  .500000E-01   1117            .9         40           200

    KSI
     1

CALCULATED PARAMETERS FOR THIS RUN

     R-P         THETA-J      BODY RADIUS PLUME RADIUS  PLUME TERM
      .501212  .970882E-02     12.7532    10618.5        106.627


     X            U/U-0         V/U-0         C-P          C-D INT

     0          .629333E-01 -.146134E-01      -.130041  -.318065E-07
      .3536     .806863E-01 -.327250E-01      -.168954   .196058E-02
      .7072     .875221E-01 -.561992E-01      -.185863   .767915E-02
     1.0608     .853983E-01 -.815108E-01      -.184733   .169564E-01
     1.4144     .761925E-01      -.107648     -.169778   .287091E-01
     1.768      .603115E-01      -.134319     -.142302   .412281E-01
     2.1216     .369774E-01      -.161372     -.101363   .522841E-01
     2.4752     .368782E-02      -.188494  -.429191E-01   .591189E-01
     2.8288    -.466128E-01      -.214377   .450951E-01   .581303E-01
     3.1824       -.139443       -.23062       .206256   .432097E-01
     3.536        -.314856       -.145877      .509298   .188863E-02



DO YOU WANT A NEW RUN?  TYPE YES OR NO.
!NO

 2290 EXIT
```

Table B.2.

```
10 DIM A$(15)
20 READ R1,R2,L,P,G9,K5,M,N,N1,K9,A0
30 DATA 1,.5,3.536,2.02,1.4,.05,.4,40,200,1,1117
40     FOR I=1 TO 13
50 READ A$(I)
60 NEXT I
70 DATA R-M,R-J,L-BETA,P,GAMMA,K,VS,M,N,N1,KSI,YES,NO
80 PRINT "DO YOU WANT INSTRUCTIONS? (TYPE YES OR NO)";
90 INPUT B$
100 IF B$=A$(13) GO TO 600
110 IF B$ = A$(12) GO TO 130
120 GO TO 80
130 PRINT "DEFAULT VALUES FOR ALL VARIABLES HAVE BEEN ASSIGNED."
140 PRINT "THEY WILL BE LISTED AFTER THESE INSTRUCTIONS."
150 PRINT "THEN YOU WILL BE ASKED WHETHER YOU WISH TO"
160 PRINT "CHANGE A VARIABLE.  AT THAT POINT TYPE IN"
170 PRINT "THE VARIABLE SYMBOL FOLLOWED BY A COMMA AND THE"
180 PRINT "VALUE YOU WISH ASSIGNED TO IT.  IF YOU TYPE"
190 PRINT "(NO, ANY NUMBER), THE RUN WILL BEGIN.  THE VARIABLE"
200 PRINT "SYMBOLS ARE AS FOLLOWS:"
210 PRINT
220 PRINT TAB(7);"R-M";TAB(20);"IS THE MAXIMUM RADIUS OF THE BODY"
230 PRINT TAB(7);"R-J";TAB(20);"IS THE RADIUS OF THE JET"
240 PRINT TAB(7);"L-BETA";TAB (20);"IS THE HORIZONTAL DISTANCE "
250 PRINT TAB(20);"BETWEEN THE POINTS AT WHICH R-M AND R-J"
260 PRINT TAB(20);"ARE MEASURED."
270 PRINT TAB(7);"P";TAB(20);"IS THE PRESSURE RATIO AT THE JET"
280 PRINT TAB(7);"GAMMA";TAB(20);"IS THE RATIO OF SPECIFIC HEATS"
290 PRINT TAB(20);"AT THE JET"
300 PRINT TAB(7);"K";TAB(20);"IS THE ENTRAINMENT COEFFICIENT"
310 PRINT TAB(7);"VS";TAB(20);"IS THE VELOCITY OF SOUND AT THE"
320 PRINT TAB(20);"STAGNATION TEMPERATURE"
330 PRINT TAB(7);"M";TAB(20);"IS THE FREE STREAM MACH NUMBER"
340 PRINT TAB(7);"N";TAB(20);"IS THE NUMBER OF STATION POINTS (X)"
350 PRINT TAB(20);"ALONG L-BETA"
360 PRINT TAB(7);"N1";TAB(20);"IS THE NUMBER OF INTEGRATION POINTS"
370 PRINT TAB(20);"ALONG L-BETA"
380 PRINT TAB(7);"KSI";TAB(20);"IS THE FRACTIONAL SAGITTAL DISTANCE"
400 PRINT TAB(20);"BETWEEN A STRAIGHT LINE BODY CURVE AND THE DESIRED"
410 PRINT TAB(20);"CIRCULAR ARC BODY CURVE.  WHEN KSI = 1, THE BODY"
420 PRINT TAB(20);"CURVE IS THE ARC OF LEAST RADIUS OF CURVATURE"
430 PRINT TAB(20);"WHICH IS TANGENT TO THE BODY AT X=0"
600 FOR I=1TO5
610 PRINT
620 NEXT I
625 PRINT "DEFAULT VALUES OF INPUT VARIABLES"
626 PRINT
630 FOR I=1TO5
640 PRINT "    ";A$(I),
650 NEXT I
660 PRINT
670 PRINT R1,R2,L,P,G9
680 PRINT
690 FOR I = 6 TO 10
700 PRINT "    ";A$(I),
705 NEXT I
710 PRINT
```

```
720 PRINT K5,A0,M,N,N1
730 PRINT
740 PRINT "   ";A$(11)
750 PRINT K9
800 PRINT
810 PRINT "NEW VARIABLE?  ";
820 INPUT B$,Z1
830 FOR I=1 TO 13
850 IF A$(I) = B$ GO TO 890
860 NEXT I
870 PRINT "VARIABLE NOT RECOGNIZED, TRY AGAIN"
880 GO TO 810
890 IF B$=A$(12) GO TO 810
900 IF B$ = A$(13) GO TO 1160
910 ON I GO TO 920,940,960,980,1000,1020,1040,1060,1080,1100,1120
920 R1=Z1
930 GO TO 1150
940 R2=Z1
950 GO TO 1150
960 L=Z1
970 GO TO 1150
980 P=Z1
990 GO TO 1150
1000 G9=Z1
1010 GO TO 1150
1020 K5 = Z1
1030 GO TO 1150
1040 A0=Z1
1050 GO TO 1150
1060 M=Z1
1070 GO TO 1150
1080 N=Z1
1090 GO TO 1150
1100 N1=Z1
1110 GO TO 1150
1120 K9=Z1
1150 GO TO 810
1160 J1=SQR((P^((G9-1)/G9)-1)*2/(G9-1))
1161 IF J1>1 GO TO 1170
1162 T=0
1163 R3=R2
1164 GO TO 1190
1170 T=SQR((G9+1)/(G9-1))*ATN(SQR((G9-1)/(G9+1)*(J1*J1-1)))-ATN(SQR(J1*J1-1))
1180 R3=R2*P^((G9+1)/2/G9)*(2/(G9+1))^((G9+1)/2/(G9-1))/J1
1190 J2=A0*J1/SQR(1+(G9-1)/2*J1*J1)
1200 R9=(R1-R2+L*L/(R1-R2))/2
1210 R9=R9*R9
1220 L9=SQR((R1-R2)*(R1-R2)+L*L)/2
1230 S9=SQR(R9)-SQR(R9-L9*L9)
1235 IF K9=0 GO TO 1285
1240 S=S9*K9
1250 R8=(S*S+L9*L9)/2/S
1260 G1=ATN(L/(R1-R2))
1270 H1=L/2-(R8-S)*COS(G1)
1280 K1=(R1+R2)/2-(R8-S)*SIN(G1)
1282 IF J1 > 1 GO TO 1285
1283 R6=123456
```

```
1284 GO TO 1290
1285 R6=(R1-R2)/(1-COS(T))
1290 H2=L+R6*SIN(T)
1310 K2=R3-R6
1320 B2=1-M*M
1330 U9=1117*M
1340 J5=J2/U9
1350 X1=0
1355 C1=0
1356 Q1=0
1360 GOSUB 3000
1370 Q1=R
1500 PRINT "INPUT VARIABLES FOR THIS RUN"
1510 PRINT
1520 FOR I= 1 TO 5
1530 PRINT "    ";A$(I),
1540 NEXT I
1550 PRINT R1,R2,L,P,G9
1560 PRINT
1570 FOR I = 6 TO 10
1580 PRINT "    ";A$(I),
1590 NEXT I
1591 PRINT"
1600 PRINT K5,A0,M,N,N1
1610 PRINT
1620 PRINT "    ";A$(11)
1630 PRINT K9
1640 PRINT
1650 PRINT "CALCULATED PARAMETERS FOR THIS RUN"
1660 PRINT
1670 PRINT "     R-P","   THETA-J","  BODY RADIUS"," PLUME RADIUS","  PLUME TERI
1680 PRINT R3,T,R8,R6,H2
1690 PRINT
1700 PRINT
1710 PRINT "     X","     R","     U/U-0","     V/U-0","     C-P","     C-D INT
1720 PRINT
1730 R8=R8*R8
1740 R6=R6*R6
1750 M1=(R2-R1)/L
1790 D1=L/N
1795 I9=N/10
1800 FOR I = 0 TO N
1805 X=D1*I
1810 I1=0
1820 X8=L/N1
1830 I2=0
1840 X1=X
1850 GOSUB 3000
1860W3=R*R*B2
1870 X1=0
1880 GOSUB 3000
1881 GOSUB 3500
1882 I1=I1+F
1884 I2=I2+G
1894 X8=L/N1
1896 IF H2<10*L GO TO 1902
1898 I5=10*N1
```

```
1900 GO TO 1920
1902 I5=H2/X8
1903 IF J1<=1 THEN I5=N1
1920 FOR I3=1 TO I5-1
1925 X1=I3*X8
1930 GOSUB 3000
1935 GOSUB 3500
1940 I4=I3/2
1945 IF (I4-INT(I4))/.5>.5 GO TO 1965
1950 I1=I1+2*F
1955 I2=I2+2*G
1960 GO TO 2010
1965 I1=I1+4*F
1970 I2=I2+4*G
2010 NEXT I3
2011 X1=(I3-1)*X8
2012 GOSUB 3000
2013 GOSUB 3500
2014 I1=I1+F
2015 I2=I2+G
2016 I1=I1*X8/3
2018I2=I2*X8/3
2020 X1=X
2030 GOSUB 3000
2040 I1=I1/2+K5*R2/4*(J5-1)/SQR(X*X+B2*R*R)
2050 I2=I2/2*B2*R-K5/4*R2/R*(J5-1)*(X/SQR(X*X+B2*R*R)+1)
2060 C=-(2*I1+I1*I1+I2*I2)
2090 S7=R-Q1
2100 C1=C1+2*3.14159*R*S8*D1*C
2190 C3=C1/3.14159/R1/R1
2195 IF I/I9-INT(I/I9)<>0 GO TO 2210
2200 PRINT X,R,I1,I2,C,C3
2210 Q1=R
2220 NEXT I
2230 FOR I=1 TO 5
2240 PRINT
2250 NEXT I
2260 PRINT "DO YOU WANT A NEW RUN?  TYPE YES OR NO.    "
2270 INPUT B$
2280 IF B$=A$(12) GO TO 810
2290 STOP
3000 IF X1>L GO TO 3020
3005 IF K9=0 GO TO 3040
3010 D2=H1-X1
3012 D3=D2*D2
3014 D4=SQR(R8-D3)
3016 R=K1+D4
3018 S8=D2/D4
3019 RETURN
3020 D2=H2-X1
3022 D3=D2*D2
3024 D4=SQR(R6-D3)
3026 R=K2+D4
3028 S8=D2/D4
3030 RETURN
3040 R=M1*X1+R1
3045 S8=M1
```

```
3050 RETURN
3500 W=X-X1
3510 W1=W*W
3520 W5=SQR(W1+W3)
3530 W4=R*SR/W5/(W1+W3)
3540 F=W4*W
3550 G=W4
3560 RETURN
```

DTNSRDC ISSUES THREE TYPES OF REPORTS

1. DTNSRDC REPORTS, A FORMAL SERIES, CONTAIN INFORMATION OF PERMANENT TECHNICAL VALUE. THEY CARRY A CONSECUTIVE NUMERICAL IDENTIFICATION REGARDLESS OF THEIR CLASSIFICATION OR THE ORIGINATING DEPARTMENT.

2. DEPARTMENTAL REPORTS, A SEMIFORMAL SERIES, CONTAIN INFORMATION OF A PRELIMINARY, TEMPORARY, OR PROPRIETARY NATURE OR OF LIMITED INTEREST OR SIGNIFICANCE. THEY CARRY A DEPARTMENTAL ALPHANUMERICAL IDENTIFICATION.

3. TECHNICAL MEMORANDA, AN INFORMAL SERIES, CONTAIN TECHNICAL DOCUMENTATION OF LIMITED USE AND INTEREST. THEY ARE PRIMARILY WORKING PAPERS INTENDED FOR INTERNAL USE. THEY CARRY AN IDENTIFYING NUMBER WHICH INDICATES THEIR TYPE AND THE NUMERICAL CODE OF THE ORIGINATING DEPARTMENT. ANY DISTRIBUTION OUTSIDE DTNSRDC MUST BE APPROVED BY THE HEAD OF THE ORIGINATING DEPARTMENT ON A CASE-BY-CASE BASIS.